THE UNIVERSITY OF QUEENSLAND

AUSTRALIA

In-situ Nanoscale TEM Observation of Cooperative Deformation Mechanisms in Nanocrystalline-Au Films

Qizhen Li

Bachelor of Material Science and Engineering

A thesis submitted for the degree of Master of Philosophy at

The University of Queensland in 2019

The School of Mechanical and Mining Engineering

Abstract

Grain boundaries activities are important for the deformation of nanocrystalline metals. Studies revealed that deformation mechanisms of nanocrystalline metals switch from dislocation-mediated regime to grain-boundary-mediated regime as approaching the "strongest" grain size. Basically, stress-driven grain growth, grain rotation and grain boundary sliding have been widely studied and discussed in the aspect of grain-boundary-mediated deformation mechanisms in nanocrystalline metals. Based on the previous studies, these grain-boundary-mediated deformation mechanisms could perform in either individual forms or cooperative forms. However, limited studies have been focused on the cooperative form mechanisms for the grain-boundary-mediated deformation mechanism, especially for the cooperative grain boundary sliding mechanisms which could lead to more ductile performance than the pure grain boundary sliding. Particularly, only a few molecular dynamic simulation studies and theoretical prediction studies investigated the cooperative grain boundary sliding mechanism in nanocrystalline metals. Therefore, it is necessary to practically examine the true deformation behaviours in straining nanocrystalline metals.

In this MPhil project, with utilising the homemade tensile device equipped with a transmission electron microscopy heating holder, in-situ transmission electron microscopy tensile tests are conducted for the magnetic-sputtering-fabricated nanocrystalline Au thin films (thickness ~ 15nm, average grain size ~ 16nm). In the in-situ experiments, the dynamic crack propagation processes of strained nanocrystalline Au films are clearly recorded under nanoscale bright-field TEM mode. It has been found that grain boundary sliding and stress-driven grain boundary migration are prevalent during the deformation processes. As cooperative deformation mechanism, stress-driven grain boundary migration assisted grain boundary sliding is confirmed experimentally. It is also found that cooperative grain boundary sliding mechanism

can be activated both at the crack tips and near the crack tips. On the other hand, the grain coalescence and active partial dislocation activities are occasionally accompanied with the cooperative grain boundary sliding mechanism during the crack tip blunting processes. Additionally, the statistics studies show that the nanotwinned grains located at the blunting crack tips tend to undergo obvious stress-driven grain growth, while the none-nanotwinned grains at the crack tips tend to slightly shrink into small size. However, the tendency of stress-driven grain growth in the nanosized grains that located at the blunting crack tips is independent to the existence of nanotwins. It is found from the statistics results that the tiniest grains (grain size < 10nm) located near the blunting crack tips tend to be totally absorbed by the adjacent larger grains.

Declaration by Author

This thesis is composed of my original work, and contains no material previously published or written by another person except where due reference has been made in the text. I have clearly stated the contribution by others to jointly-authored works that I have included in my thesis.

I have clearly stated the contribution of others to my thesis as a whole, including statistical assistance, survey design, data analysis, significant technical procedures, professional editorial advice, financial support and any other original research work used or reported in my thesis. The content of my thesis is the result of work I have carried out since the commencement of my higher degree by research candidature and does not include a substantial part of work that has been submitted to qualify for the award of any other degree or diploma in any university or other tertiary institution. I have clearly stated which parts of my thesis, if any, have been submitted to qualify for another award.

I acknowledge that an electronic copy of my thesis must be lodged with the University Library and, subject to the policy and procedures of The University of Queensland, the thesis be made available for research and study in accordance with the Copyright Act 1968 unless a period of embargo has been approved by the Dean of the Graduate School.

I acknowledge that copyright of all material contained in my thesis resides with the copyright holder(s) of that material. Where appropriate I have obtained copyright permission from the copyright holder to reproduce material in this thesis and have sought permission from co-authors for any jointly authored works included in the thesis.

Publications included in this thesis

No publications included.

Submitted manuscripts included in this thesis

No manuscripts submitted for publication.

Other publication during candidature

1. Liu, Shi-Jian, Zou, Yi-Chao, Shi, Xiao-Lei, **Li, Qi-Zhen**, Yang, Yu-Zhe, Liu, Wei-Di, Chen, Zhi-Gang and Zou, Jin (2018). Vapour-solid growth of MoxW1-xTe2 nanobelts by a facile chemical vapour deposition method. Journal of Alloys and Compounds 777 926-930.

Contributions by others to the thesis

Prof. Jin Zou and Dr Lihua Wang designed the project and discussed the project results with me. Dr. Mung Teng Soo and Dr. Graeme Auchterlonie instructed me to operate transmission electronic microscopy.

Statement of parts of the thesis submitted to qualify for the award of another degree

No work submitted towards another degree have been included in this thesis.

Research Involving Human or Animal Subjects

No animal or human subjects were involved in this research.

Acknowledgement

First of all, I must express the highest gratitude toward Professor Jin Zou and Professor Lihua Wang who designed this project and are continuously providing helpful guidance for my two-year period MPhil research. Secondary, I must show my appreciations toward Professor Xiaolu Pang and Professor Jiao Teng who assisted me in the nc-Au thin films fabrication of my project. Thirdly, I must greatly thank to Doctor Mun Teng Soo who patiently guided me to learn transmission electron microscopy. Fourthly, I also thank to all the friends from Professor Jin Zou's group as well as the colleagues from my office who provided useful personal opinions for my project.

Besides, I must simultaneously show my appreciations and respect to my parents. They are always behind me, supporting me, caring for me and giving me huge motivations. In the meantime, I must sincerely thank to Chloe Li who mentally supported me even when I was depressed and frustrated during setbacks and failures.

Finally but not the last, thanks to the University of Queensland and Australian Research Council. Without the provided laboratories and equipment, this thesis couldn't be achieved.

Financial support

No financial support was provided to fund this research.

Key Words

In-situ nanoscale TEM experimental observations, deformation mechanisms, grain-boundaries-mediated mechanisms.

Australian and New Zealand Standard Research Classifications (ANZSRC)

ANZSRC code: 100712, Nanoscale Characterization, 40%

ANZSRC code: 100716, Nanofabrication, Growth and Self-Assembly 40%

ANZSRC code: 091207 Metals and Alloy Materials, 20%

Fields of Research (FoR) Classification

FoR code: 0912, Materials Engineering, 50%

FoR code: 1007, Nanotechnology, 50%

Table of Contents

LIST OF FIGURES & TABLES

List of Abbreviations used in the thesis

nc	nanocrystalline
GB	grain boundary
GBs	grain boundaries
cg	coarsened grain
FCC	face centred cubic
TEM	transmission electron microscopy
HR	high resolution
BF	bright field
DF	dark field
NBDP	nano-beam diffraction pattern
SAEDP	selected area electron diffraction pattern
TJs	triple junctions
PVD	physical vapour deposition
RF	ratio frequency

Chapter 1. Introduction

1.1 Introduction

Deformation mechanism investigations on metals are critically important as they can help metallurgical engineers design and manufacture metal products with greater performance. Basically, full dislocations are one of the most prevalent media for plastic deformation of metals since full dislocation glides can directly lead to plastic deformation[1-5]. However, easy and excessive full dislocation glides can cause metals to show weak strength performance. To strengthen metals, approach of grain refinement strengthening (alternatively called grain boundary strengthening) is utilised to restrain full dislocation glides[1-5]. Based on dislocation pile-ups deformation mechanisms, grain boundaries (GBs) are excellent pinned obstacles for impeding full dislocation glides.[1-5] Full dislocations will stop gliding while encountering GBs, resulting in full dislocations pile-ups in the front of GBs[1-5]. This sort of strengthening approach can be directly indicated by conventional Hall-Petch formula: the yield strength of metals are enhanced as the grain size are reduced into smaller scale[1-5].

In recent decades, nanocrystalline (nc) metals are attractive to researchers due to their superior mechanical performances and unique deformation mechanisms compared to their bulk, coarsen-grain (cg) counterparts. Studies revealed that the "strongest" grain size existed for nc-metals, in which the nc-metals show the strongest yield strength peformance[6-9]. This means that while reducing the grain size to be smaller than the strongest size, nc-metals will become softer than the strongest strength. Showing phenomenon against the conventional Hall-Petch formula, the nc-metals softening phenomenon can be stated as inverse Hall-Petch effect[10-12]. On the other hand, deformation mechanisms are also different for the nc-metals near the strongest grain size (statistically d~ 10~30nm) [13-17]. Studies revealed that full dislocations pile-ups mechanism played minor roles for nc-metals because limited full dislocations initially pre-exist inside the grains of nc-metals. Meanwhile, full dislocations are also very difficult to

nucleate and multiply in the nanosized grains[6-9,13,15,17-19]. In contrast, partial dislocations mediated mechanisms[20-30] and GBs-mediated mechanisms[12,17,31-70] are more activated in the deformation processes of nc-metals. Especially, GBs-mediated deformation mechanisms can relatively dominate the deformation processes of nc-metals in the inverse Hall-Petch effect regime, since in this super-tiny grain size regime, the volume of GBs accounts for a relatively larger proportion of total volume in the nc-metals. In this scenario, GBs-mediated mechanisms are thought to be detrimental for the nc-metals strength performance.

Basically, grain rotation[36,40,42,45,47-51,56-60], stress-driven grain growth[31,32,37-40,42,43,46,47,49,50,53,55,56,59,61-64] and GB sliding[17,41,44,55,65-70] are mainly investigated in the of GBs-mediated mechanisms regime. Computer simulation studies and theoretical calculation prediction studies suggested that GBs-mediated deformation mechanisms are able to perform individually, or alternatively cooperate and accommodate with each other in the deformation processes of nc-metals. However, most experimental observation studies only observed that pure GBs-mediate mechanism individually dominated the deformation processes. For example, pure grain rotation mechanism has been confirmed by Shan et al[58] in d~10nm nc-Ni, pure stress-driven GB migration mechanism has been confirmed by Wang et al[59] in d~18 nm nc-Au and pure GB sliding mechanism has been confirmed by Kumar et al[68] in d~30 nm. In the aspect of cooperative mechanisms, limited studies such as by Wang et al[35,59] confirm that grain rotation can cooperate and accommodate with stress-driven grain growth during the tensile deformation processes of nc-Pt and nc-Au, consistent with the previous results of computer simulations and theoretical predictions. However, so far cooperative GB sliding mechanism proposed from computer simulations and theoretical predictions is yet to be confirmed by direct experimental observations.

Thus, more in-situ experimental observations should be aimed at studying the cooperative mechanisms in nc-metals, especially for the cooperative GB sliding mechanism. Basically, a

number of experimental observation studies revealed that pure GB sliding are prevalent in nc-metals which can easily nucleate nanocracks and cause nc-metals to be brittle[71-76]. In contrast, a few studies predicted that cooperative GB sliding can enhance the fracture toughness in nc-metals[63,64,77]. After reviewing these different and contradictive views from the studies, it is necessary to make clear the cooperative GB sliding mechanisms in experimental conditions to provide guidance for metal designs.

1.2 Outline

I organized the thesis in the following pattern. Chapter 1 is an overview of the study background and the scope of unsettle issues. Chapter 2 reviews some basic knowledge of crystal defects and the previous investigations on the deformation mechanisms of nc-metals, mainly the GBs-mediated mechanism such as grain rotation, stress-driven grain growth and GB sliding plus some dislocation-mediated mechanisms. Chapter 3 gives details on preparation work prior to in-situ tensile experiments (including steps to prepare experiment samples), pre-characterization of the fabricated nc-Au thin films and methodology of in-situ TEM experiments. Chapter 4 analyses and discusses the results of the in-situ experiment results, and finally Chapter 5 summaries the discussed results plus depicted the future outlook of the project.

Chapter 2. Basic Knowledge & Literature Review

2.1 Basic Knowledge: Full Dislocations & Shockley Partial Dislocations, Stacking Faults & Twins and Grain Boundaries

Dislocations are important deformation media for most of the metals. Full dislocations can be naturally pre-existed in metals or nucleated from Frank-Read sources to maintain the plastic deformation processes[78]. Activated full dislocations tend to glide in the perfect forms: a line of atoms move for integral multiple units of Burger's vector[1-4].

Taking face-centered-cubic (fcc) crystal structure metals as illustrations because the fcc-structured nc-Au thin films are used as investigation object in this study. Basically, fcc-structured metals naturally have closed-pack directions $<\bar{1}10>$ and closed-pack planes $\{111\}$[1-5]. Full dislocation tends to glide on closed-pack planes in the closed-pack directions because of lowest energy requirement[1-5]. Burger's vector of full dislocations is $\frac{a}{2}<\bar{1}10>$[1-5]. However, sometimes full dislocations do not glide in the perfect forms with Burger's vector $\frac{a}{2}<\bar{1}10>$, instead dislocations can partially glide in a smaller unit with Burger's vector $\frac{a}{6}<\bar{1}2\bar{1}>$ or $\frac{a}{6}<\bar{2}11>$[5]. This can be regarded as disassociation of full dislocations, which is $\frac{a}{2}<\bar{1}10> = \frac{a}{6}<\bar{1}2\bar{1}> + \frac{a}{6}<\bar{2}11>$. As a consequence, Shockley partial dislocations will generate. Full dislocation disassociation can take place while satisfying the *Frank's Energy Criterion*[5]: dislocation energy must decrease after the full dislocation disassociations. Fundamentally, dislocation energy can be roughly estimated by formula $E_{total} \approx G*b_2$. For example, as full dislocation disassociates into Shockley partial dislocations: for perfect full dislocation $\vec{b} = \frac{a}{2}<\bar{1}10>$, dislocation energy= $G*a^2/2$; for Shockley partial dislocations, dislocation energy=$G*a^2/6$. In this scenario, apparently, total dislocation energy is becoming lower, resulting in the phenomenon of full dislocation disassociation. In the fcc-structured metals, family of $\frac{a}{2}<\bar{1}10>$

full dislocations and their corresponding disassociated Shockley partial dislocations can be summarized in the model of the Thompson tetrahedron[79].

The simplest stacking faults are generated by Shockley partial dislocations glides. For example, the normal stacking order '…ABCABC…' of fcc-structured metal close-packed {111} planes will switch to '…ABC**ACA**BCA…' stacking order by one unit of Shockley partial dislocations glide. Stacking faults can also be extended to be wider by more units of partial dislocations glides. On the other hand, stacking fault energy (γ) indicates the extra energy per unit area of stacking fault. Based on some theoretically calculated studies[80-85], table 1 shows intrinsic the staking fault energy (γ_{isf}) values of the commonly-investigated metals. In the previous decades, it was believed that metals with low γ_{isf} tended to emerge partial dislocation activities because of easier full dislocation disassociations[5]. However, some recent studies revealed that partial dislocation activities not only depend on γ_{isf} but also unstable stacking fault energy (γ_{usf})[86,87]. Simply, unstable stacking fault energy γ_{usf} is defined as the lowest potential energy barrier for full dislocations nucleation. In this case, with the improving modification, the ratio γ_{isf} / γ_{usf} can be utilised as a reference to predict the deformation mechanisms of metals. While ratio γ_{isf} / γ_{usf} approaching 1, full dislocation activities are more favourable than partial dislocation activities.

Twinning consists of extensions of stacking faults, the stacking order of twinning is in '…ABCA**B**ACBA…' symmetric order. As the extension of stacking faults, twin activities are highly related to partial dislocation activities. Moreover, studies revealed that the induced twins can enhance mechanical performances such as strength[88,89], hardness[90,91], fracture toughness[88,89] and anti-fatigue[92].

Grain boundaries (GB) are a type of planar defects which help separate the grains with different crystalline orientations[93]. Basically, deformation processes related to GBs can be stress-driven and diffusional, both of which can induce grain growth. Inducing more GBs (grain refinement) can strengthen the metals since GBs are obstacles for full dislocations in the deformation processes. However, if GBs account for a large ratio of the total volume (the average grain size is sufficiently small), GBs activities will take the place of full dislocation activities and dominate the deformation processes.

Table 1.1 Conclusive intrinsic staking fault energy values (γ_{isf}) for metals.

Metal Type	γ_{isf} [mJ/m2]
Pt	308[84]
Pd	161[81], 194[82]
Ni	125[83], 154[84], 155[80], 180[81]
Al	124[81], 144[80], 160[83]
Cu	48[84], 70[80,81], 73[83]
Au	33[84], 34[85], 36[85], 37[85], 44[81], 55[83]
Ag	17[84], 20[83], 33[81]
Co	20[80]

2.2 Dislocation-mediated & Twinning Mechanisms

Transgranular full dislocations become less important in nc-metals (especially the grain size is smaller than the strongest size) because few full dislocations pre-exist in the minimum-sized grains. Meanwhile, few Frank-Read dislocation sources can exist to nucleate full dislocations in the deformation processes. All these factors contribute to the rare existence of full dislocations in nc-metals. However, in-situ TEM observation studies by Wang et al[94,95] revealed that full dislocation activities are still existent in the deformation processes of nc-Pt

thin films, even in the d~10nm Pt grains. Figure 2.1 are high-resolution (HR) TEM images that show the full dislocations nucleation and annihilation processes during the tensile deformation processes[92]. Grain A (d~12 nm) was monitored during the whole deformation processes, as labelled by white dash lines in Figure 2.1a. A full dislocation dipole (labelled "1" "2") pre-existed in the grain A (shown in Figure 2.1a), subsequently it moved toward each other (shown in Figure 2.1b~c) and annihilated at localized tensile stress (shown in Figure 2.1d). With further tensile straining, new full dislocations (labelled "3" "4") emitted from GBs of grain A (shown in Figure 2.1e) and full dislocation "5" nucleated inside grain A. With further tensile straining, full dislocation "4" "5" annihilated (shown in Figure 2.1f) and full dislocation "3" slowly moved inside the grain A (as shown in Figure 2.1f~h). In the in-situ observation experiments, Wang et al even observed active full dislocations activities in the d<10 nm nc-Pt grains. As shown in Figure 2.1e, generation of full dislocations in the minimum-sized nc-Pt grains can come from the rapid association of Shockley partial dislocations emitted from GBs.

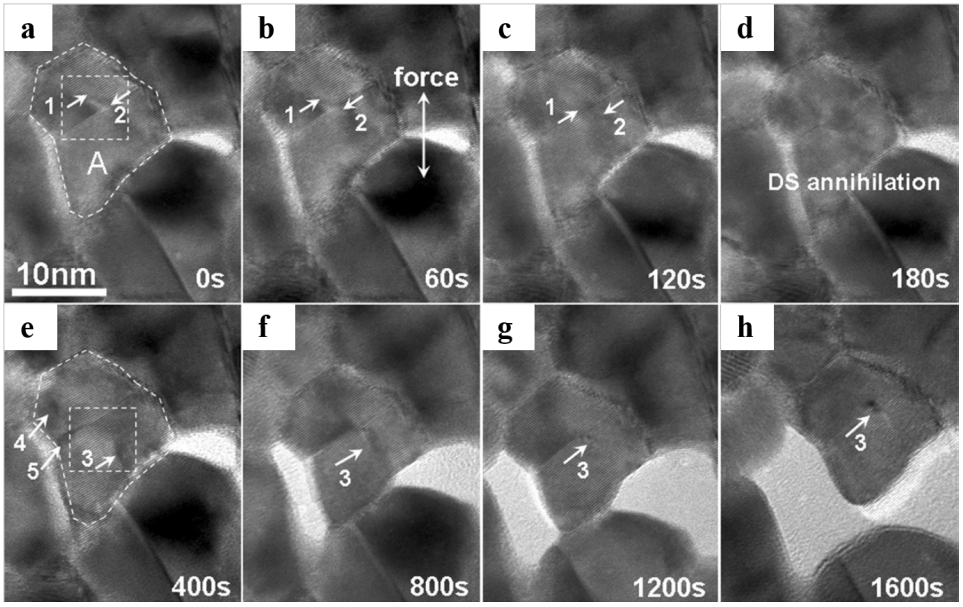

Figure 2.1 Full dislocation activities of a d~12nm Pt-grain A during the tensile straining process. (a~d) Annihilation process of a full dislocation dipole named "1" "2". (e) Full dislocations named "4" "5"emitted from GBs and full dislocation named "3" nucleated inside the Pt-grain A. (f) Full dislocations "4" "5"annihilated. (f~h) Full dislocation "3" slowly moved inside grain A.[92]

Compared to full dislocations, more attentions are paid to the partial dislocations activities in nc-metals (with d<15nm). MD simulation studies by Swygenhoven et al[13,86] and Yamakov's et al[24,26] show that partial dislocations can emit from GBs during straining. Particularly, Swygenhoven et al[86] concludes that the subsequent activities of GBs-emitted partial dislocations in nc metals can be either partial dislocation extension (in low γ_{isf} investigated-metals) or partial dislocation evolved into full dislocations (in high γ_{isf} investigated-metals) in terms of γ_{isf} values of investigated metals. Experimentally, Liao et al[22] studied the deformed nc-Cu (low γ_{isf}) specimen via ex-situ HRTEM observations that partial dislocations emitted from GBs which further extended and evolved into twining in the deformation processes. Meanwhile, no full dislocation was found in the deformed nc-Cu specimen.

Deformation twinning are always observed and investigated in the deformation of nc-metals. Some statistical studies discovered that the number of deformation nanotwins apparently increases in the deformed nc-metals after severe plastic deformation[96,97]. It was also discovered that the existence of nanotwins can effectively enhance nc-metals mechanical performance [88-92]. On the other hand, a large number of studies emphasized on the deformation mechanisms of twining formation, which are already comprehensively reviewed in both cg-metals[98] and nc-metals[25]. Simply, pole mechanism[99], prismatic glide mechanism[100] and faulted dipole mechanism[101] are the fundamental deformation mechanisms of twinning in cg-metals, in which full dislocation sources are essential to activate the mechanisms. Differently, deformation mechanisms of twining in nc-metals are relied on the partial dislocation activities. Overlapping (accumulation) of two stacking fault ribbons via partial dislocations slip on adjacent planes is a simplest way to form twinning nucleus[21,102,103]. In this mechanism, intra-grain and GBs are positions to form twining nucleus. Moreover, thick twin lamellas were observed to be pinned single end on the GBs and then continuously extended inside grain. However, due to high

energy requirement, partial dislocations are difficult to naturally nucleate on every single adjacent slip plane for accumulative twinning growth. Thus, it is believed that this sort of accumulative twinning formation is via successive Shockley partial dislocation emissions from GBs which overlap on the adjacent slip planes[104,105].

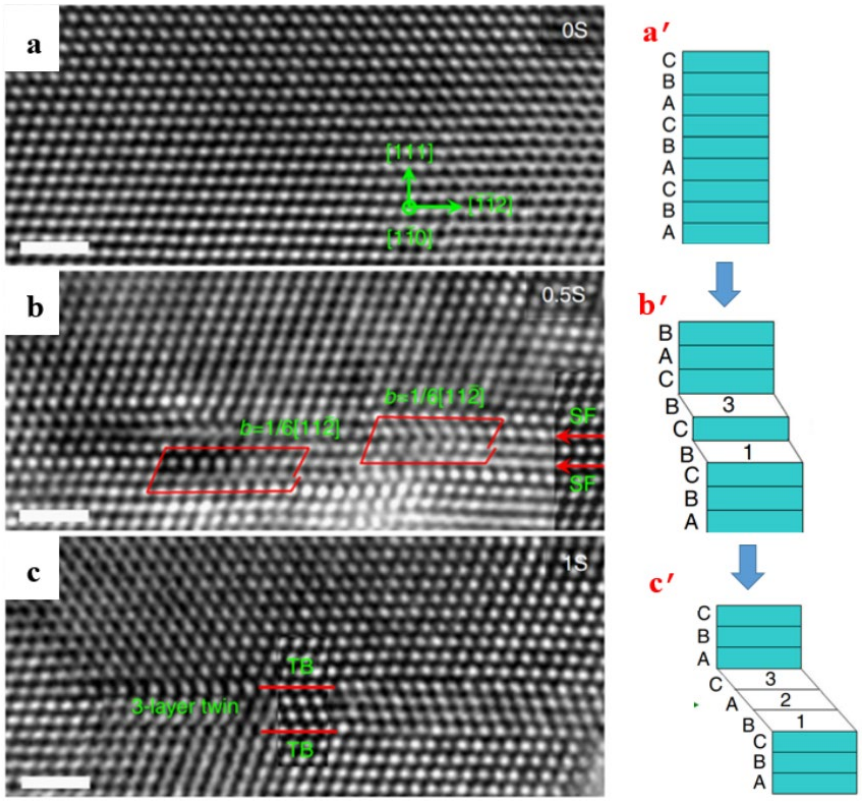

Figure 2.2 Nucleation process of a simplest three-layer twin nucleus in nc-Pt sample, shown by in-situ HRTEM images (a~c) and their corresponding schematic diagrams (a'~c'). (a) & (a') Elastic deformation stage of sample, no partial dislocation was seen. (b) & (b') 0.5s later, two partial dislocations nucleated during plastic deformation, between which there was a single atomic layer interval. (c) & (c') Another 0.5s later, another partial dislocation nucleated between previously-nucleated partial dislocations, finally a three-layer twin nucleus formed.[106]

Most observed and proposed twining mechanisms in nc-metals basically followed the 'layer-by-layer partial dislocations overlapping' deformation processes. Interestingly, Wang et al[106] recent in-situ observed a novel mechanism for twining formation rather than "layer-by-layer" mechanism. Figure 2.2 exhibits a series of enlarged in-situ HRTEM images, indicating the novel twining formation mechanism. As shown in Figure 2.2a, at the beginning, no partial

dislocation was observed in the nc-Pt grain. With further straining, two partial dislocations nucleated, as shown in Figure 2.2b. It was observed that these two partial dislocations were separated by an atomic unit. With further straining, another partial dislocations nucleated in the middle of the previously-nucleated partial dislocations; consequently, a twin nucleus formed via overlapping of these partial dislocations, as shown in Figure 2.2c. Schematic diagrams of this novel twin formation process are in Figure 2.2a'~c' to help understand the deformation process. In this study, Wang et al mentioned that this twin nucleus formation process should be more plausible than "layer-by-layer" deformation process because this novel twinning formation mechanism is more energetically favoured than "layer by layer" deformation mechanism (lower twinning fault energy required).

2.3 GBs-mediated Deformation Mechanisms

2.31 Grain Rotation

Grain rotation was firstly in-situ observed by Hackney et al while comparing the HRTEM lattice fringe angle changes between adjacent grains in the straining nc-Au samples[36]. The in-situ straining HRTEM characterization is one of the most convincing approaches to investigate grain rotation. Similarly, Wang et al[35] clearly observed that the lattice mis-orientation between nc-Pt grains (d~6 nm) can rotate from high angle to low angle, as an accommodated way for grain coalescence process. In this study, Pt nanograin tilted, rotated and finally coalesced with the adjacent grain after GB annihilated, as shown in Figure 2.3. To obtain better understandings on this process, Figure 2.3a'~d' are schematic diagrams corresponding to Figure 2.3a~d, respectively. As shown in Figure 2.3a, at the beginning, lattice fringes of grain 1 could not be captured because grain 1 was not in the low zone axis at the moment. With vertical tensile straining, lattice fringes of grain 1 "appeared" due to self-tilting, as shown in Figure 2.3b. At the moment, lattice orientation difference between grain 1 and grain 3 was 12.6°. With further straining, the lattice orientation of grain 1 rotated to be almost parallel with the lattice

orientation of grain 3, as shown in Figure 2.3c. At the moment, grain 1 and grain 3 were still separated by the GB. But with further straining, the GB between grain 1 and grain 3 eventually annihilated and the entire coalescence process between these two Pt grains finalized, as shown in Figure 2.3d. Grain coalescence is a sort of the stress-driven grain growth mechanisms in the deformation of nc-metals, which will be introduced in the next sub-chapter.

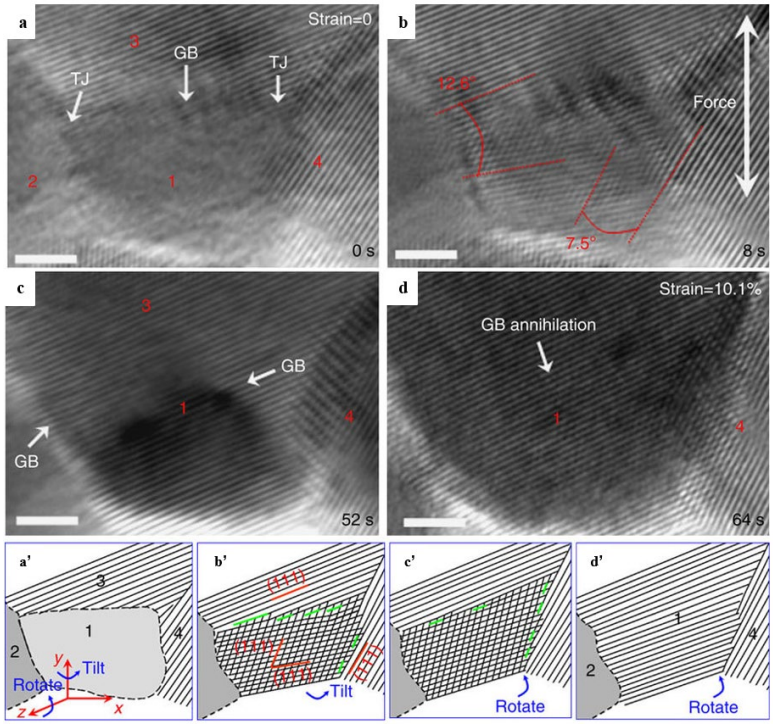

Figure 2.3 In-situ observation of grain coalescence process in nc-Pt between grain 1 and grain 3 via grain tilting (b), grain rotation(c) and GB annihilation (d) step by step. Schematic diagrams a'~d' corresponds to a~d, respectively.[35]

As shown in Figure 2.3, grain tilting and grain rotation successively took place to accommodate the grain coalescence process. Generally, grain tilting was regarded as a unique sort of grain rotation, which can be directly indicated by observing the changing contrast in TEM bright field (BF) mode or dark field (DF) mode. Meanwhile, to further confirm the grain tilting, localized diffraction patterns are required. This contrast observation method was utilised in the study by Wang et al[56], as the contrast of grain G changed from dark to white, as shown in Figure 2.4a~c. To further verify this transformation of contrast in grain G contribute by grain

tilting rather than sample distorting, method of nano beam diffraction patterns (NBDP) were utilised. Apart from grain G, grain R was also monitored during the straining. While comparing the NBDPs of grain R during straining (shown in Figure 2.4R1~R3), we can see minimum change among the images, indicating that the entire straining sample was not distorting. In contrast, while comparing the NBDPs of grain G during straining (shown in Figure 2.4G1~G3), we can see that the patterns significantly changed. Thus, combined these two series of NBDPs, it has been confirmed that grain G experienced self-tilting during the deformation process. Based on this approach, Shan et al[57] and Jin et al[42] utilised TEM-DF mode rather than BF-mode to in-situ observe and confirm grain rotation (tilt) in straining nc-Ni and nc-Al, respectively.

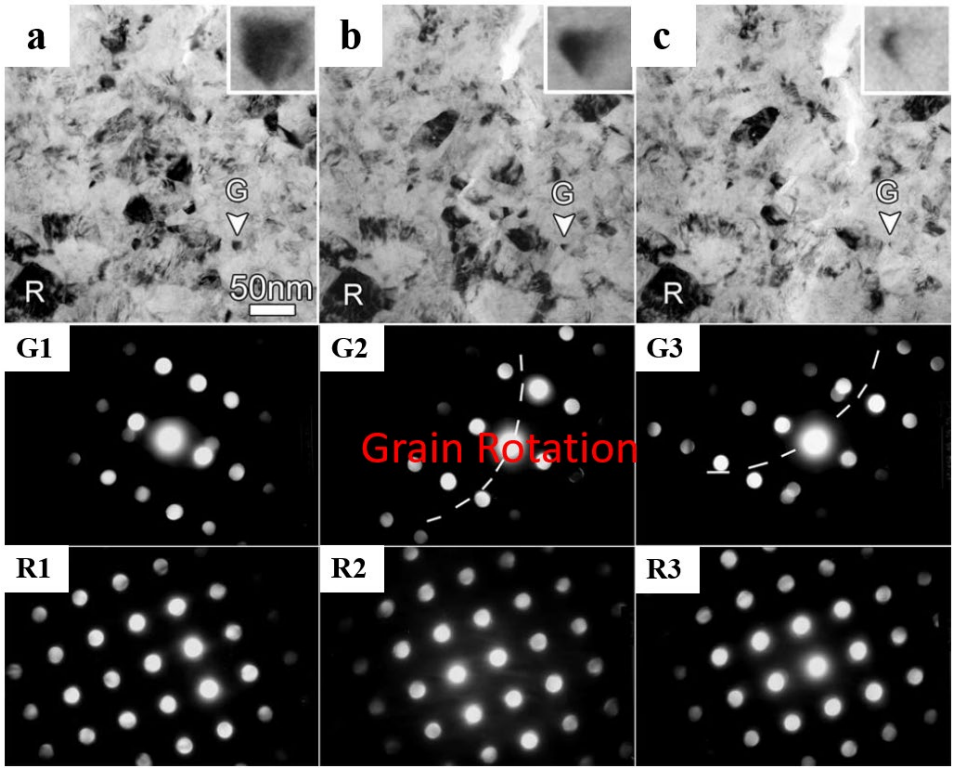

Figure 2.4 Nc-Ni grain G was tilting during the deformation as the contrast of grain G changed from dark to white (a~c), verified by NBDPs in images G1~G3. The entire deformation sample was stable while comparing to the simultaneously unchanged NBDPs of grain R (shown in images R1~R3).[56]

2.32 Stress-driven Grain Growth

Fundamentally, grain growth can take place spontaneously at high temperature due to rapid atomic diffusions[107]. With applying external stress, grain growth can also be achieved in nc-metals at relatively low temperature. In this fashion, it is defined as "stress-driven grain growth". One representative study of stress-driven grain growth was shown by Zhang et al[46] that nc-Cu can be mechanically coarsened even at liquid-nitrogen temperature. Obviously, deformation mechanisms of stress-driven grain growth at low temperature are different from grain growth at high temperature by atomic diffusion. Previously-reviewed in Figure 2.3, we already know that stress-driven grain growth can be accomplished by grain coalescence process via deformation processes of stress-driven grain tilting, grain rotation and GBs annihilation. More similar grain rotation/tilting and grain coalescence processes are in studies from Wang et al[61], Jin et al[42] and Shan et al[57].

Concretely, stress-driven grain growth can also be accomplished by stress-driven GB migration and twin-assisted grain growth. Especially for stress-driven GB migration, it is prevalent under tensile, compressive or cyclic loading in nc-metals. For example, Farkas et al[32] reported GB migration in ultra-fined nc-Ni from MD simulation results that grain size and grain shape of nc-Ni (d~6nm) constantly changed during the tensile deformation (at 12% strain, grain size increased by 2.5 nm). In experimental observations, Sharon et al[108] revealed that grain size of nc-Pt thin films increased to be doubled at only 2% strain of tensile deformation which is caused by stress-driven GB migration. Interestingly, Mompiou et al[109] in-situ observed that stress-driven GB migration can even be performing in submicron scale Al grains. In this study, however, stress-driven GB migration was an associated mechanism for the dislocation-mediated mechanisms since full dislocation nucleation and partial dislocation emission from GBs were far dominating than GB-mediated mechanisms.

Theoretical studies indicated that rapid GB diffusional rate assist the stress-driven GB migration processes in nc-metals. Thus, metallic nanofilms are ideal materials for in-situ observations of stress-driven GB migration because GB diffusional processes can be greatly enhanced in 2D-nanofilms. For example, Wang et al[59] exhibited a series of in-situ HRTEM images that clearly demonstrates the stress-driven GB migration in nc-Au thin films. As shown in figure 2.5, smaller grains (G2~G5) were gradually absorbed by the adjacent larger grains (G1 and G6) in the both sides via stress-driven GB migration during the tensile deformation process. Initially in Figure 2.5a, six adjacent grains (G1~G6) were found at a crack tip. Their boundaries were traced by using white dashed lines. With tensile straining, the crack tip was propagating. As the result, shown in Figure 2.5b~f, GBs of G1 and G6 expanded inwardly, and absorbed the G2~G5 eventually. Moreover, Wang et al also observed that stress-driven GB migration and grain rotation can cooperate and accommodate with each other to induce further grain growth.

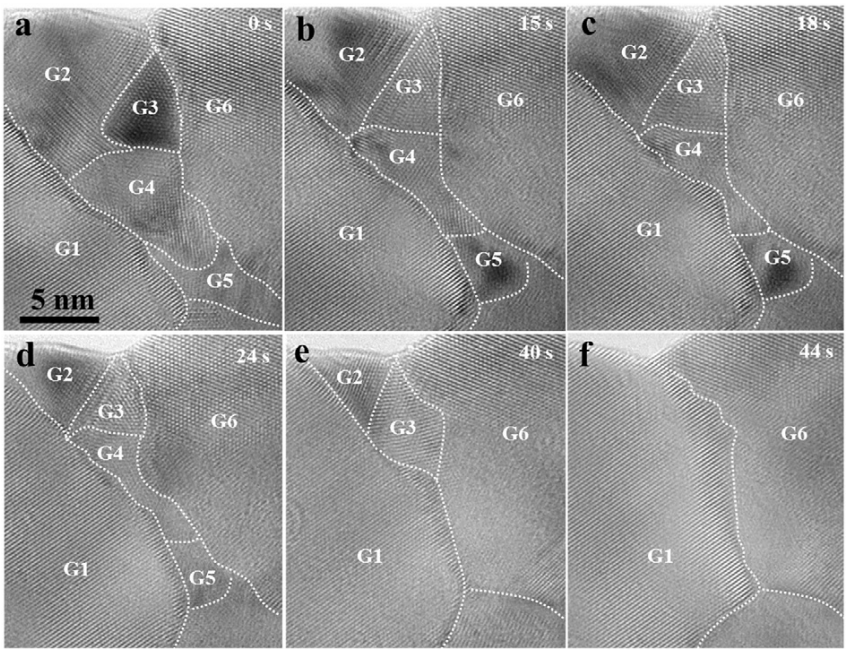

Figure 2.5 Dynamic in-situ HRTEM images demonstrate stress-driven GB migration (0s ~ 44s) at the crack tip during deformation. In this deformation process, smaller grains G2~G5 (in the middle) were gradually and eventually absorbed by their adjacent larger grains G1 and G6.[59]

Interestingly, GB migration process was also discovered in nanoparticles. Revealed by Jong Min Yuk et al[110], GB migration is one of the mechanisms observed in the process of Au nanoparticle coalescence. Differently, no external stress was applied on the Au nanoparticles. This Au nanoparticle spontaneous coalescence process was accomplished by the rapid GB diffusional migration processes.

Furthermore, twin-assisted grain growth mechanism is a novel discovery in the deformation investigation of nc-metals. In terms of the study by Luo et al[111,112], increasing numbers of nanotwins were formed in the deformation processes of nc-Au thin films after cyclic loading to fatigue. With HRTEM characterization of nanotwin formation processes in nc-Au, it was observed that the grain growth can be accomplished by mutual twin extension between adjacent grains. This process ultimately led to coalescence of the adjacent grains, which became a larger nanotwinned-grain. As shown in Figure 2.6, schematic diagrams of twin-assisted grain growth mechanism was proposed, illustrating the specific deformation processes observed in the HRTEM experimental observations. The subsequent study by Pan et al[92] explained that nanotwinned Cu is extremely stable under long-term cyclic loading. Thus, twin-assisted grain growth could be a beneficial mechanism for enhancing anti-fatigue performance of nc-metal.

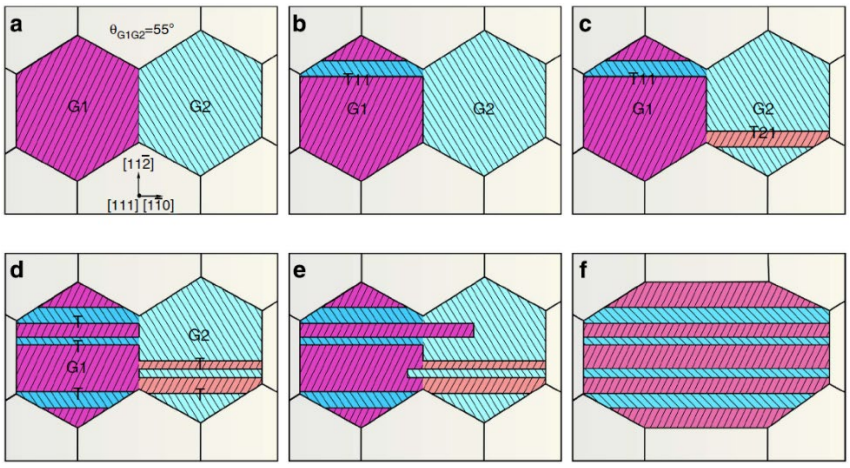

Figure 2.6 Proposed schematic illustrations of nanotwin-assisted grain growth mechanism, based on the results of in-situ HRTEM observation.[109]

2.33 Grain Boundary Sliding

Grain boundary (GB) slidings are activated in cg-metals at ultra-slow strain rate deformation and high temperature, displaying as creep deformation[113]. On the other hand, GB sliding can also be activated in straining nc-metals at room temperature. GB slidings in nc-metals were widely studied by MD simulations. Schiøtz et al[8,9] discovered that softening phenomenon (inverse Hall-Petch relation) emerged in the smallest size nc-Cu mainly because of the extensive GB slidings. Besides, Swygenhoven et al[41] also revealed the prevalent GB slidings (via atomic shuffling and stress-assisted free volume migration) in the MD-simulated deformation processes of d~12 nm grain size nc-Ni model.

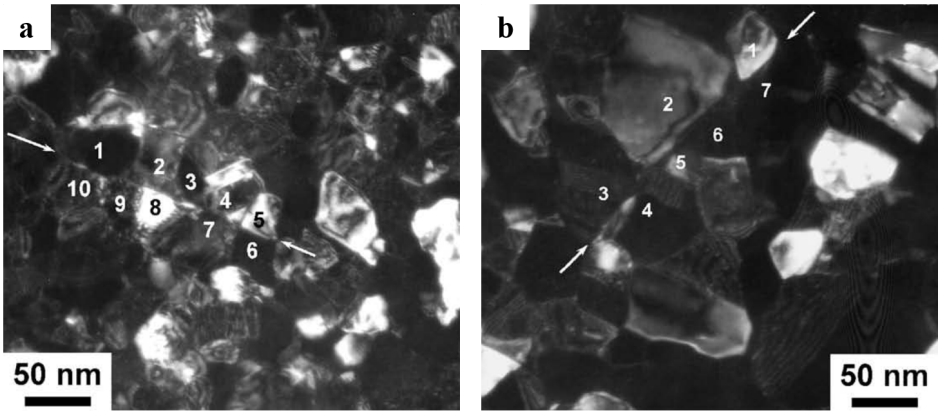

Figure 2.7 Observations of grain alignments, the indicator for GB slidings in deformed nc-Pd sample.[47]

In the experimental observation aspect, both ex-situ and in-situ TEM characterization results validated the pure GB sliding in nc-metals. In ex-situ experiments, grain alignment is an indicator reflecting activated GB slidings in straining nc-metals. Figure 2.7 are post-mortem TEM images, indicating GB slidings can be activated. As shown in Figure 2.7a & b, both sides of grains in nc-Pd are orderly arranged and separated by straight-line GBs[47]. It is beneficial for GB slidings to arrange in this order, and thus GB slidings can perform smoothly. This grain alignment phenomenon was also observed in dynamic in-situ characterization, revealed by Sergueeva et al[69]. During tensile experiments at elevated temperature (750℃), NC Ni_3Al grains

were aligned instantaneously within 1 seconds. With another approach, Kumar et al[68] in-situ observed crack blunting deformation processes in nc-Ni and confirmed the pure GB slidings, whereas a number of nanocracks nucleated during the pure GB slidings so that the nc-Ni fractured rapidly.

2.4 Cooperative GB Sliding

Having reviewed some individual types of deformation mechanisms in nc-metals, a widely-discussed cooperative deformation mechanism, cooperative GB sliding (CGBS), should be noticed. CGBS means that more than one deformation mechanisms are involving in and accommodating with the GB slidings during the deformation processes in nc-metals rather than pure GB slidings. So far, a majority of studies related to CGBS are contributed by MD simulations and theoretical modellings[33,63,64,69,77]. No direct experimental observation ever clearly confirms the CGBS mechanism at the room temperature or at the slightly elevated temperature.

Compared to CGBS mechanism, frequent pure GB slidings can be detrimental for the mechanical performances of nc-metals because nanocracks always nucleate at triple-junctions (TJs) during pure GB slidings which will promote rapid nc-metals frature. Recent experimental observations of pure GB sliding can refer to Hosseinian et al[70]. This study in-situ observed and compared the deformation behaviours of the thinner and the thicker nc-Au films (30nm thick vs 100 nm thick). For the deformation processes of 30 nm nc-Au films, nanocracks frequently nucleated at TJs due to excessive pure GB sliding, which rapidly evolved into some sub-propagating cracks and promoted rapid frature. In contrast, multi-slips were observed in the 100nm thick nc-Au films, indicating the higher ductility than the 30nm thickness ones.

In terms of proposed CGBS models, a few deformation mechanisms can potentially accommodate with GB slidings. With these accommodated mechanisms, fewer nanocracks

would nucleate during the GB sliding processes. The model proposed by Sergueeva et al[69] described the possible cooperation between GB sliding and other mechanisms, as shown in Figure 2.8. Based on the in-situ experiments and some previous studies, grain rotation, grain coalescence, stress-driven GBs migration and intergranular shearing are most likely to create grain alignment condition for GB slidings (example was shown in Figure 2.7).

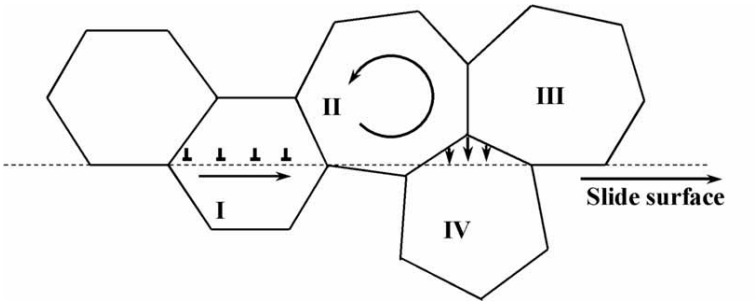

Figure 2.8 Schematic illustrations of the proposed CGBS model, GB sliding could be accommodated by several deformation mechanisms. Grain I: intergranular shearing. Grain II: grain rotation & grain migration. Grain III & IV: pure grain migration.[69]

Intergranular shearing is a type of deformation mechanism rarely observed in straining nc-metals. One example is as shown in Figure 2.9[47]. With localized tensile stress, a single grain was sheared and exhibited intra-grained displacement. Mediated by full dislocations, intergranular shearing can only be achieved in relatively larger grains (d~50nm, shown in Figure 2.9).

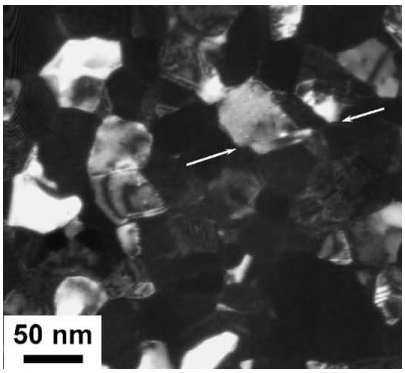

Figure 2.9 Observation of intergranular shearing deformation. It's a sort of possible accommodated mechanisms for GB sliding in compression-torsion mode deformation of nc-Pd sample.[47]

2.5 Deformation Mechanisms Investigations of nc-Au Thin-films

Nc-Au thin film (thickness less than 100 nm) is a type of two-dimensional materials different from bulk nc-Au counterparts. Deformation mechanisms can be significantly different in two-dimensional nanomaterials due to large ratio of surface-volume. In the past two decades, there are a number of experimental studies investigating deformation mechanism of nc-Au thin films. In 1993, Milligan et al[114] in-situ characterized the bending processes of nc-Au thin film (d~ 8~25 nm), indicating that the secondary nanocracks nucleated ahead of the main cracks before intergranular shearing took place between these cracks. Later in 1995, Milligan et al[36] further observed grain rotation in brilliant plasticity (strain~30%) nc-Au thin films (thickness ~ 10~20 nm, d~10 nm). Meanwhile, no dislocation activities were found in this study. In 1998, Harris et al[45] revealed that highly-random grain rotation was also prevalent in 250℃ annealed nc-Au thin films (thickness~25nm, d~66 nm). It was suggested it caused by GB diffusion.

No more progressive studies on the deformation mechanisms of nc-Au thin films until the time goes to 2011. Liu et al[34] in-situ observed that the grain rotation was prevalent in the adjacent grains near cracking tips in nc-Au thin films (thickness~20 nm, d~20nm). In this study, it was discovered that three dislocations nucleated near a low angle GB and formed a wedge disclination, which could be a compensation mechanism for grain rotation. In 2014, Luo et al[111] revealed a new deformation mechanism that nanotwins prevalently formed under cyclic tensile loading in nc-Au thin film (thickness~20 nm, d~19 nm). Proposed explanation model has been previously shown in Figure 2.6. In 2017, Wang et al[59] in-situ observed that stress-driven GB migration was prevalent in the deformation processes of nc-Au thin films (thickness~10nm, d~15nm). In this study, observed stress-driven GB migration processes were activated between large grains, and also between large grains and small grains. Meanwhile, grains rotation can also be an accommodated mechanism for stress-driven GB migration. Moreover, active dislocation behaviours were also observed in some larger grain (d>20nm). Based on all the in-

situ HRTEM results, Wang et al[59] made a statistics on the relationship between grain size and deformation mechanisms in nc-Au thin films, as shown in Figure 2.10. It can be discovered from the sketched graph that GBs-mediated mechanisms are much more prevalent than dislocations activities in the nc-Au grains with grain size smaller than 15nm.

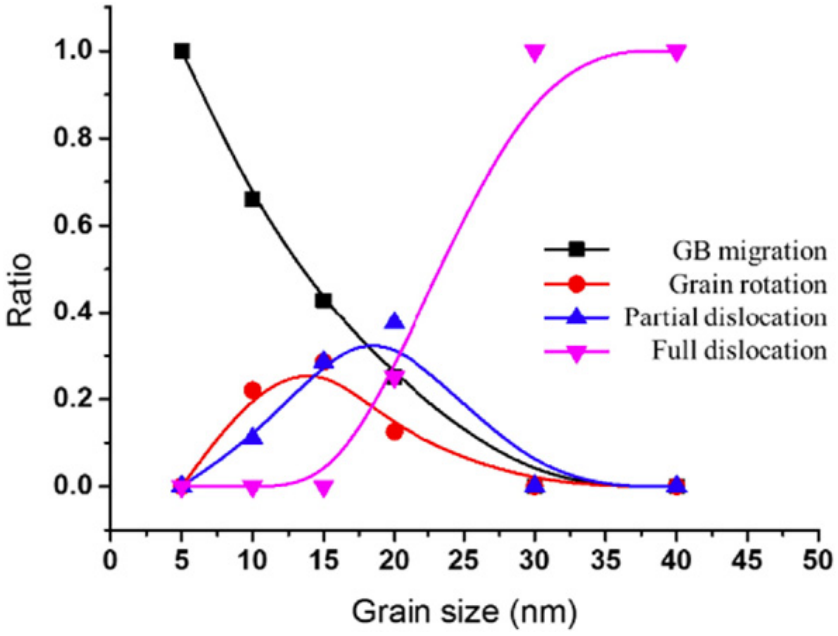

Figure 2.10 Relationship of grain size and deformation mechanisms in nc-Au thin films based on in-situ observations.[59]

Chapter 3. Experiment Preparation & In-situ Experiments Methodology

3.1 Fabrication of nc-Au Thin Films via PVD

Nc-Au thin films are fabricated by magnetic sputtering, which is a sort of the physical vapour deposition (PVD). As shown in Figure 3.1, its working mechanism is very simple. The sputtering gas is argon. Argon ions (Ar^+) and the electrons generate via argon atoms collide with electric-field accelerated electrons. Under the dual-performances of electric field and magnetic field, motion of electrons are restrained within the specific areas, which can increase the collision chances with sputtering argons. Then, these Ar^+ ions are accelerate by electrical field and bombard the surface of Au target, causing Au atoms to bounce upward which finally deposit onto the NaCl substrate that locates at the top of machine.

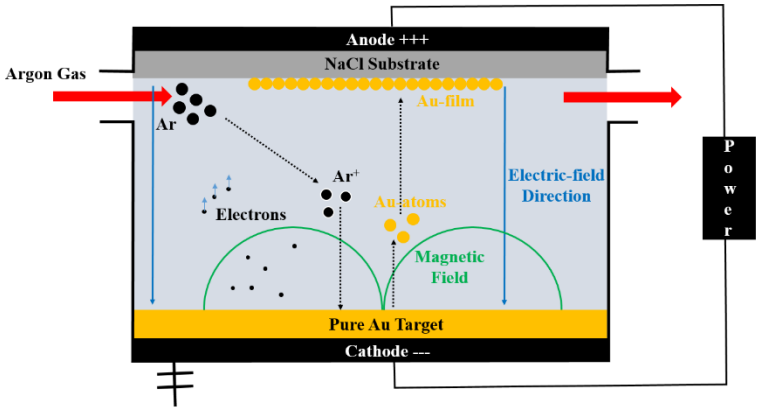

Figure 3.1 Schematic diagram of magnetic sputtering process. With this method, nc-Au thin films were obtained by sputtering from the bottom Au target to the top NaCl substrates.

Two sorts of magnetic sputtering can be primarily used: direct current (DC) magnetic sputtering and ratio frequent (RF) magnetic sputtering. DC magnetic sputtering is a good choice for metal targets, thus it was mainly used for fabricating my nc-Au thin films. Some parameters must be strictly followed to obtain the nc-Au thin films with ideal thickness and average grain size. Sputtering power is a critical parameter in the magnetic sputtering, after

several experimental trials I found that 20W (4%) the right value to harvest nc-Au thin films with average grain size below 20nm. To deposit these 15nm thick TEM transparent thin films, deposition time can't be too long: ideally, I controlled deposition time to be around 3 minutes long.

3.2 Pre-characterization of the Nc-Au Thin-films

To better understand the features of the PVD-fabricated nc-Au thin films, TEM pre-characterizations are necessary before in-situ TEM experiments. As shown in Figure 3.2, we can know some fundamental information about the fabricated nc-Au thin films. Figure 3.2a shows that the nc-Au grains are hexagonal and homogeneously distributed. Inset at the right bottom is the selective area electron diffraction pattern (SAEDP) for the nc-Au. The diameter of each diffraction ring has been measured, and the subsequent calculation results show that these diffraction rings accurately correspond to the planes of fcc-Au (200), fcc-Au (111), fcc-Au (220) and fcc-Au (311). On the other hand, grains size statistics in the Figure 3.2b shows the distribution of grain size of the fabricated nc-Au thin films. As can be seen in the Figure 3.2b, a majority of nc-Au grains are in the range of 5~25 nm, and the average grain size is approximately 16.4 nm.

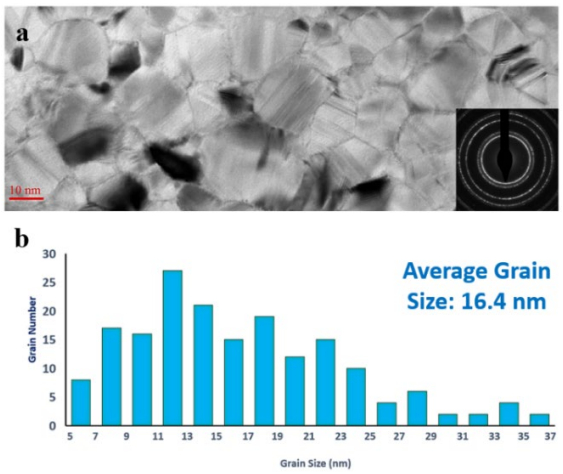

Figure 3.2 Bright field TEM characterization (a) and grain size statistics (b) for the fabricated nc-Au thin films. (a) A majority of grains appeared as hexagonal shape and homogenously distributed. Inset at the right bottom is

its selective area electron diffraction pattern. (b) Apart from image (a), more grains were included into the statistics. Finally, the average of grain size was figure out to be approximately16.4 nm.

To show the comprehensive view of the fabricated nc-Au thin films, more TEM images of various resolutions are also shown in Appendix 1. It can be clearly observed from Appendix 1 that there are very few nanocracks and nanovoids pre-existed in the fabricated nc-Au thin films, which are beneficial to the crack propagation observations in the subsequent in-situ TEM straining experiments.

Figure 3.3 is an enlarged HRTEM image of the fabricated nc-Au. As can be seen, 3 of 4 measured mis-orientations of lattice arrangement between the adjacent grains are larger than 15° (10°, 20°, 23° and 26°, respectively). Based on such observations, we can anticipate that most nanosized grains in the nc-Au thin films are separated by high angle GBs.

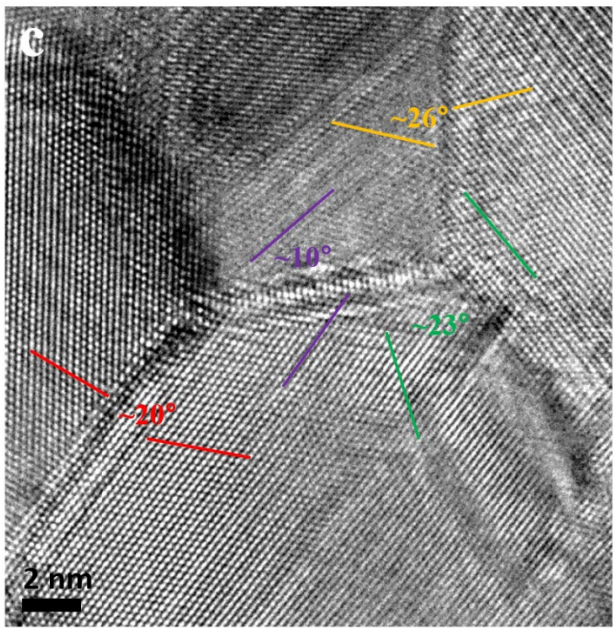

Figure 3.3 HRTEM characterization (700kx magnification) of the fabricated nc-Au thin film. Measured lattice mis-orientations between adjacent grains were 10°, 20°, 23° and 26°, respectively, indicating that a majority of grains of fabricated nc-Au thin films were separated by high-angle GBs.

3.3 In-situ Tensile Tests with Homemade Bimetallic-strips TEM Device & TEM Heating-holder

To conduct tensile tests inside a TEM, I utilized the homemade bimetallic strips grid to equip with the Gatan TEM heating holder. As shown in Figure 3.4, the bimetallic strips grid consists of two identical bimetallic strips and a 3-mm diameter metallic ring. Bimetallic strips are fixed in the opposite directions on the 3-mm metallic ring. Generally, the metallic ring can be made of Cu or Mo. Each bimetallic strip is made of two different layers of alloys: $Mn_{72}Ni_{10}Cu_{18}$ and Fe-Ni_{36} alloys, respectively. These two alloys have a large mismatch in the thermal expansion coefficient: 26×10^{-6} K^{-1} and 2.9×10^{-6} K^{-1}, respectively. While elevating the testing temperature, the two alloys of the bimetallic strips can have a large mismatch in the thermal-expansion elongation, which in return causes the bimetallic strips to extend outwardly. Thus, in this way, the bimetallic strips can act as tensile actuators to perform tensile test for the attached nanofilms inside a TEM. The dynamic deformation processes of the straining nanofilms can be recorded by the TEM CCD camera.

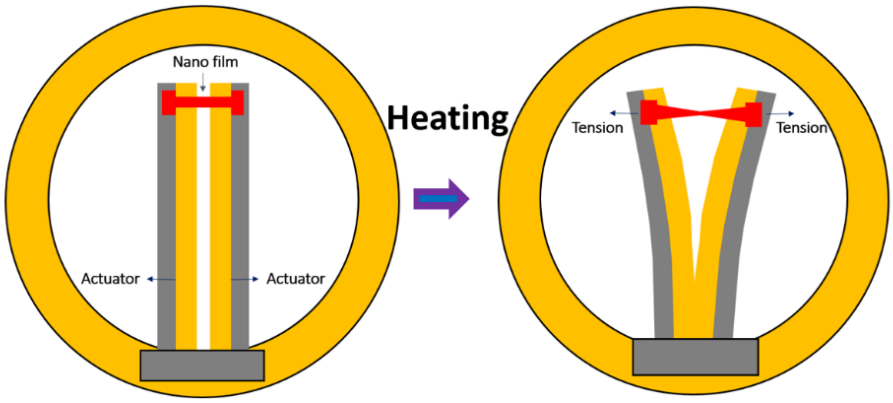

Figure 3.4 Schematic diagrams of the homemade bimetallic strips grid utilized for performing tensile tests inside a TEM. The nanofilms were attached on the bimetallic strips. While elevating the experiment temperature, the bimetallic strips will extend outward. As the result, the attached nanofilms were undergoing tensile deformation.

Manufacture approach for the homemade TEM tensile test device will be introduced step by step in the following, simply with the illustrations shown in Figure 3.5:

1. Polishing the 3-mm diameter metallic ring and bimetallic strips (shown in Figure 3.5a) on 2000 abrasive paper, and then cleaning them in an ultrasonic washing machine with acetone bath.
2. Placing the paraffin and a clean glass sheet on the heating stage, then turning on the heating stage and waiting for the paraffin melted.
3. Smearing a small amount of melted paraffin onto the heated glass sheet, and placing the bottom of the metallic ring onto the melted paraffin, as shown in Figure 3.5b. Subsequently, gently lifting the glass sheet away from the heating stage. Paraffin will cool down quickly so that metallic ring will be firmly fixed on the glass sheet.
4. Mixing AB glue (epoxy resin) by ratio 1:1 (shown in Figure 3.5c) on another clean glass sheet. Then, using a "needle" (shown in Figure 3.5c) to smear a small amount of mixed-glue to one side of bimetallic strips, and fixing the metallic strips on the bottom of the metallic ring in the opposite direction.
5. Adjusting the distance between two bimetallic strips. Must make sure the separating gap is small enough (approximately 2~10 μm) by observing it under optical microscopy.
6. Placing the glass sheet with the bimetallic strip grid in a dry environment for 2 days, allowing the glue to be fully solidified (shown in Figure 3.5d).
7. After 2 days natural drying, glue will be totally solidified. At the moment, placing the glass sheet onto the heating stage (elevated temperature must be controlled below 100 °C). While the paraffin melted, picking up the bimetallic grid with a tweezer.
8. Cleaning out the remaining paraffin with acetone bath in an ultrasonic machine. What should be noticed is that cleaning time must not exceed 3 minutes because acetone is harmful to the solidified AB glue.

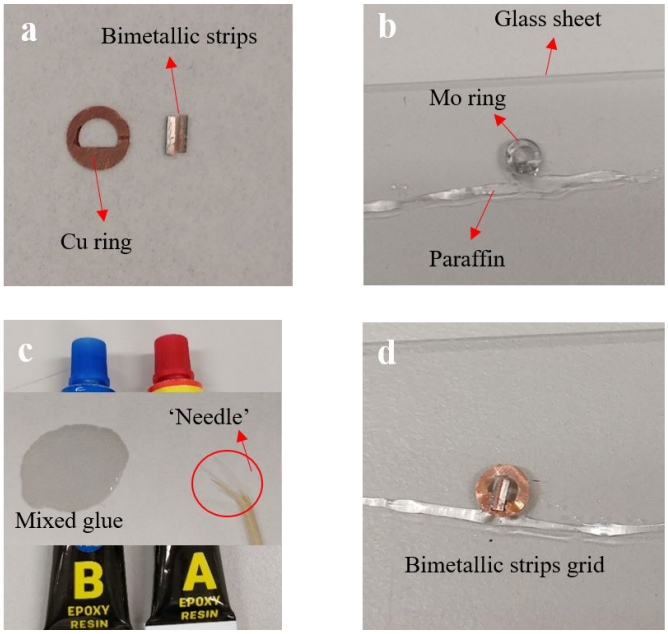

Figure 3.5 Steps for manufacturing the homemade bimetallic strip grid. (a) Metallic Cu ring and bimetallic strips have been polished by the sand paper. (b) Metallic Mo ring was fixed on glass sheet by paraffin. (c) AB-glue was mixed for fixing bimetallic strips onto the metallic ring, inset shows the wooden needle for smearing the mixed AB-glue. (d) A bimetallic strips grid that was drying naturally in lab environment for 2 days.

3.4 Preparation Steps of Transferring Nc-Au Thin-films to Bimetallic Strips Grids

Fabricated nc-Au thin film needs to be attached onto the homemade bimetallic strips grid before transferring bimetallic strips grid into the TEM heating holder. Here are the detailed preparation steps:

a. Obtaining a clean knife blade and a TEM tweezer, then washing them in the ultrasonic washing machine with ethyl alcohol bath.
b. Washing the bimetallic strips grid in the ultrasonic washing machine with ethyl alcohol bath.
c. Naturally drying the knife blade, tweezer and bimetallic strips grid on the clean filter papers.

d. Placing the top side of the fabricated nc-Au film (with Au film surface) into the side position (vertical state) and firmly fixing the nc-Au film by clipping its corner with tweezer, then cutting the nc-Au film from top to bottom with the knife blade.

e. Repeating step (d) until the nc-Au film is finally cut into 5mmx5mm surface dimensions.

f. Removing the 5mmx5mm nc-Au films from the NaCl substrates by placing the substrates into the distilled water. In this way, the nc-Au films can float freely on the distilled water, as shown in Figure 3.6a. ***Notice: the tweezer must clip the substrate part of the nc-Au films while transferring them into distilled water, otherwise the nc-Au films will be damaged.***

g. Transferring the floating nc-Au films to attach the bimetallic strips grid by picking them up from the distilled water. The middle tip of the bimetallic strips must be aligned with the floating nc-Au films.

h. Using a small piece of filter paper to absorb the water in the bimetallic strips grid, and then placing it onto another piece of filter paper and letting it dry naturally.

i. Placing the bimetallic strips grid under optical microscope, observing it that if there undamaged Au film can be seen between bimetallic strips (like bridges, as shown in Figure 3.6b).

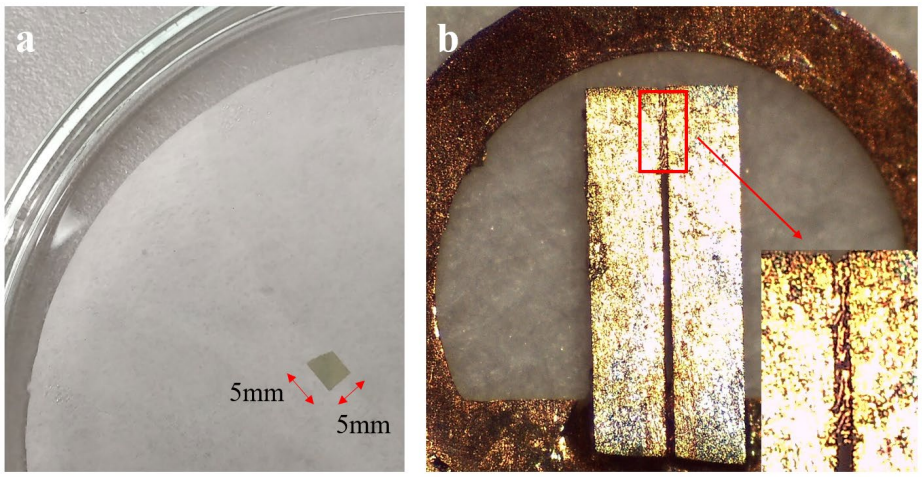

Figure 3.6 (a) The 5mm x 5mm configuration nc-Au film was floating on the water. (b) After transferring the nc-Au film from the water to be on bimetallic strip grid, the nc-Au film can be firmly attached to the bimetallic strips.

Above are the detailed steps for preparing a bimetallic strips grid sample from the fabricated nc-Au thin films. It's simple but needs practises and repetitions to make some perfect samples for in-situ tensile tests. Picking floating nc-Au films from water is the most skilful part in the sample preparation processes since Au films must be transferred to sit on the tip position of the bimetallic strips. Also, it needs essential care while drying the grid by filter paper water-absorbing because the attached nc-Au films can be easily damaged by the tension in the water.

3.5 TEM Heating Experiments

Figure 3.7 shows the equipment used for performing in-situ TEM heating experiments. Figure 3.7a exhibits a Gatan 652 heating holder that is fixed in the fixation stage. The bimetallic strips grid should be placed in the area which is highlighted by red dashed lines, as shown in Figure 3.7b. Prior to placing the bimetallic strips grid into the heating holder, at least 30 minutes time of plasma cleaning is a must-required step for the heating holder, for the sake of cleaning out the carbon film attached on the heating holder. Meanwhile, after the bimetallic strips grid is placed into the heating holder, another 1 minute time of plasma cleaning is also required for the heating holder. Figure 3.7c shows that the TEM heating holder has been already inserted into the Tecnai F20-TEM. The heating holder has been connected to the heating stage controller by the connector. The heating stage controller is highlighted by orange dashed lines, and more details are as shown in Figure 3.7d. The heating holder is switched into manually-controlled mode. The heating experiment will start while adding the input current manually. In this way, the heating rate can be manually controlled by adjusting the input current. Thus, the strain rate of the deformation process can be finely controlled to be 10^{-6} s^{-1}~10^{-3} s^{-1}. In the heating experiments, in order to minimize the thermal influence, the testing temperature is suggested not to exceed 80°C.

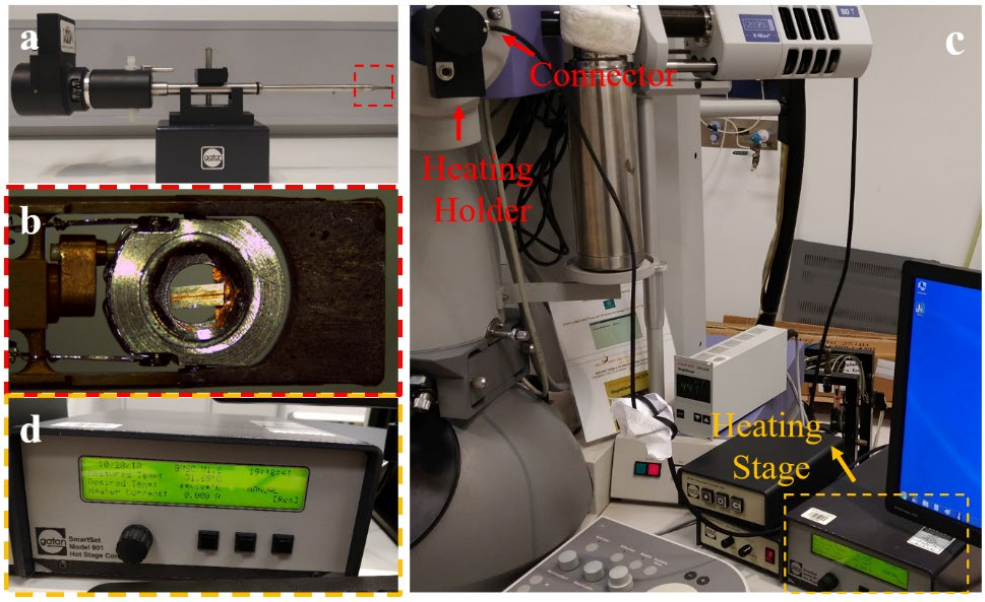

Figure 3.7 Equipment for TEM heating experiments. (a) The Gatan heating holder is fixed on the stage, the red-dashed-lines highlighted area is the position for placing bimetallic strips grid. (b) More details for the red-dashed-lines highlighted area, the bimetallic strips grid is fixed in the heating holder. (c) The heating holder is inserted in the F20-TEM and connected to the heating holder controller with the connector. The heating controller is highlighted by orange dashed lines at the right bottom of the image. (d) More details for the orange-dashed-lines highlighted area. During the heating experiments, the heating controller was switched into manual current control mode.

Chapter 4. Results & Discussion

Figure 4.1 is a set of bright-field (BF) TEM images taken from a nanostructured Au film, captured during deformation process, and presents an overview of the crack propagation process between two main cracks - crack 1 at the top left and crack 2 at the bottom right of the images. Figure 4.1a shows the initial state, in which the nano-sized grains are named as "G1~G10" to track their subsequent evolution during the formation. For convenience, $GB_{i\text{-}j}$ is defined as the grain boundary between Gi and Gj. As shown in Figure 4.1a, the crack 1 has already blunted along tensile direction on G2. With further tensile loading and crack blunt, a nanocrack is nucleated at the triple junction of G2, G3 and G4, as shown in Figure 4.1b (highlighted as red arrow). Based on the previous studies[71,72,74-77], excessive GB sliding can

lead to the nucleation of nanocracks, and in turn leading to rapid fracture. In Figure 4.1b, a new crack tip is initiated at GB_{8-9}. In Figure 4.1c, crack 1 rapidly propagates through connecting the nanocrack, resulting in a crack tip propagates on G5. With further loading, Figure 4.1d shows the crack tip on G5 blunts as GB sliding take place at G_{4-5} that is parallel to the tensile direction. On the other hand, the tip of crack 2 continuously propagates along the GB_{8-9}. In Figure 4.1e, more crack 1 blunt on G5 is witnessed through the GB sliding along the GB_{4-5}. Interestingly, the crack tip of crack 2 propagates and reaches to G6, then the crack tip blunts on G6 is seen through the GB sliding along the GB_{6-9}. With continuing the tensile loading, as shown in Figure 4.1f, more GB sliding can be seen with crack 1 through GB_{4-5} and crack 2 through GB_{6-7}. Towards to the end of crack propagation process (refer to Figure 4.1g and Figure 4.1h), there are more GB slidings between GB_{4-6} for both crack 1 and 2, and eventually the breakage take place by the separation of G4 and G6. As shown in Figure 4.1, extensive GB slidings have been observed during the deformation and the crack propagation. In this deformation process, only one nanocrack has nucleated (refer to Figure 4.1b), suggesting the nanostructured Au film has a good plasticity at slow strain-rate deformation. It is of interest to note that, during the deformation, the shape/size of the many grains are constantly changed (e.g. G4~G8 and G10), also some nanosteps generated such as marked by red arrows in Figure 4.1h, indicating that stress-driven GB migration process is also occurred in accompany with the GB sliding.

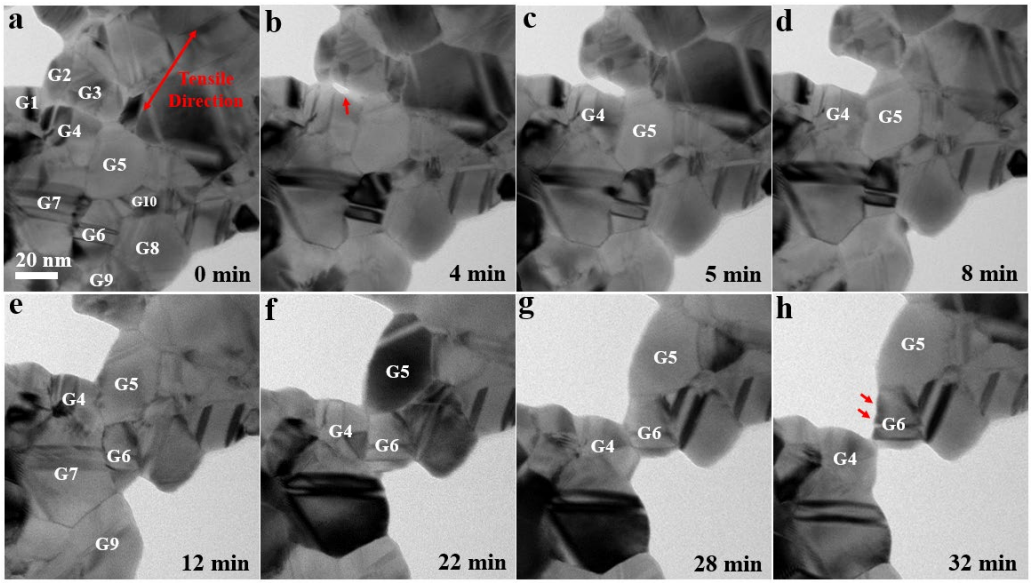

Figure 4.1 In-situ nanoscale observation of a crack propagation process between two main cracks (crack 1 at the left top and crack 2 at the right bottom, respectively). GB slidings and stress-driven GB migration are active in this deformation process. (a~c) A nanocrack nucleates at TJ among G2~G4 due to excessive GB sliding, causing that the crack 1 directly propagates through $GB_{3\text{-}4}$ to G5. (d~e) Continuous GB slidings are along $GB_{4\text{-}5}$, causing continuous blunts in crack 1. (f~h) More continuous GB slidings are along $GB_{4\text{-}5}$, $GB_{4\text{-}6}$ and $GB_{6\text{-}7}$, finally this localized nc-Au film fractures after G4 separates with G6.

To understand the relationships between stress-driven GB migration and GB sliding, it is further investigated the structural change during the deformation through investigating the enlarged TEM images. Figure 4.2 is a set of enlarged TEM images exacted from the crack propagation process in Figure 4.1. Figure 4.2a shows the crack tip of crack 1 propagates to G5, and the crack tip of crack 2 is propagating through the $GB_{8\text{-}9}$. To track the size/shape changes of G5, its boundary is traced by using the white dashed lines in Figure 4.2a. With tensile loading, GB sliding take place along the $GB_{4\text{-}5}$, as shown in Figure 4.2b. Simultaneously, the size/ shape of G5 are changed, its boundary is traced by a yellow dash line. The comparison of both dash lines shown in Figure 4.2b indicates that (1) $GB_{4\text{-}5}$ moved towards the upper left of image, leading it to be parallel with tensile direction and benefit GB sliding; (2) the relative changes of $GB_{4\text{-}5}$ is approximately 15° clockwise (marked by red arrow); (3) G5 is expanding longer

along the tensile direction by absorbing G4, G6 and G7. Thus, it is confirmed that the GB sliding along GB_{4-5} is accompanied with stress-driven GB migration. Particularly, without nucleating any visible nanocrack during the deformation, the stress-driven GB migration is acting as an assisted accommodation beneficial for ductile GB sliding. With further loading, it is observed more stress-driven GB migration assisted GB slidings along GB_{4-5} in Figure 4.2c. Simultaneously, the crack tip of crack 2 blunts via GB sliding between G6 and G9. As shape/size of G6 is changed during the GB sliding, this deformation process is also assisted by stress-driven GB migration. With continuing the loading, GB sliding direction along GB_{4-5} is changed to be relatively vertical, as shown in Figure 4.2d (red arrow). Meanwhile, immediately following the GB sliding of G5 along GB_{4-5}, G6 is also sliding upwards along GB_{6-7}, relatively G7 is sliding downwards along GB_{6-7}. In Figure 4.2e, more GB slidings are along GB_{4-5}, GB_{4-6} and GB_{4-7}, and finally G4 is only connecting to G6, as shown in Figure 4.2f. Details of the shape/size changes of G5 and G6 before and after GB sliding in Figure 4.2 are as shown in Figure 4.3. By comparisons, the shape/size of G5 becomes longer/larger after GB sliding, as the shape of G6 becomes more round but it roughly maintains the same size after GB sliding. Thus, it is confirmed that GB sliding at the crack tips along GB_{4-5} and along GB_{6-7} in Figure 4.2 are both assisted by stress-driven GB migration. These observations are consistent with the theoretical studies and simulation studies previously mentioned in the literature review chapter. In those studies, the stress-driven GB migration assisted GB sliding mechanism at the crack tips are more energetically favoured than pure GB sliding, which can significantly enhance the fracture toughness in nc-metals[63,64].

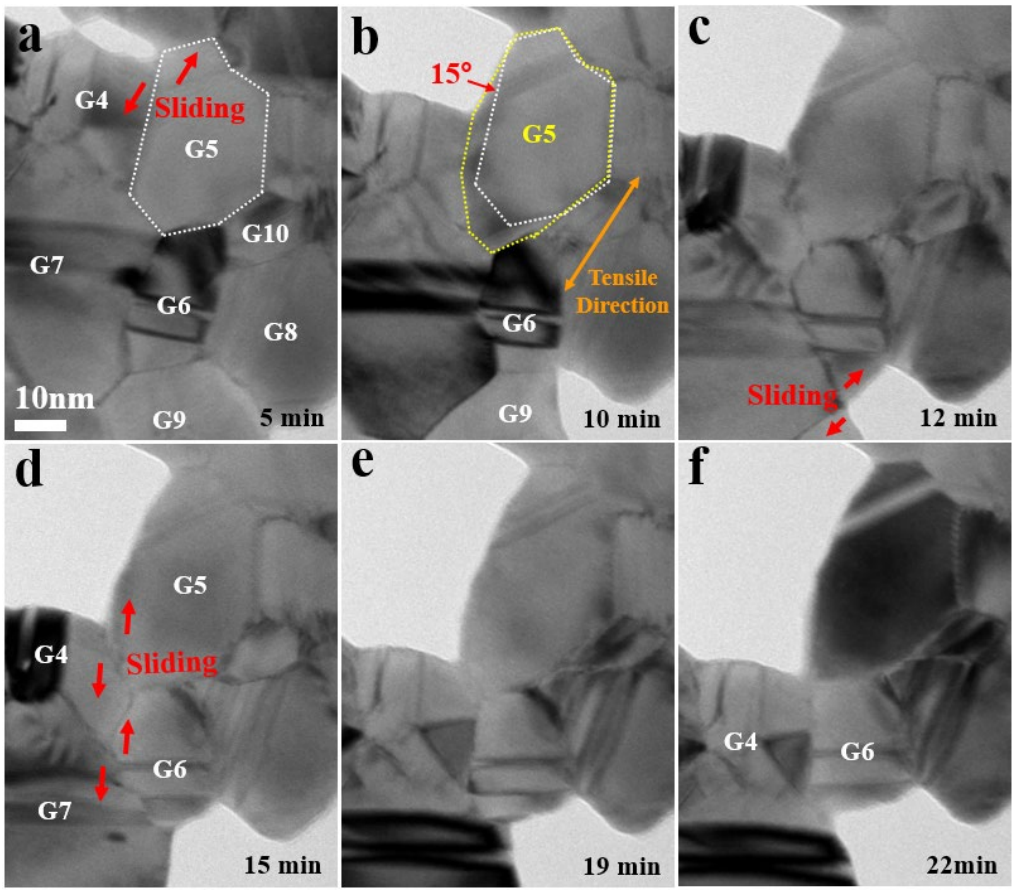

Figure 4.2 (a~b) In-situ observations of stress-driven GB migration assisted GB slidings along $GB_{4\text{-}5}$. (c) Besides in-situ observations of continuous stress-driven GB migration assisted GB slidings along $GB_{4\text{-}5}$, more GB slidings are along $GB_{6\text{-}9}$. (d~f) More in-situ observations of stress-driven GB migration assisted GB slidings are simultaneously along $GB_{4\text{-}5}$, $GB_{4\text{-}6}$ and $GB_{6\text{-}7}$.

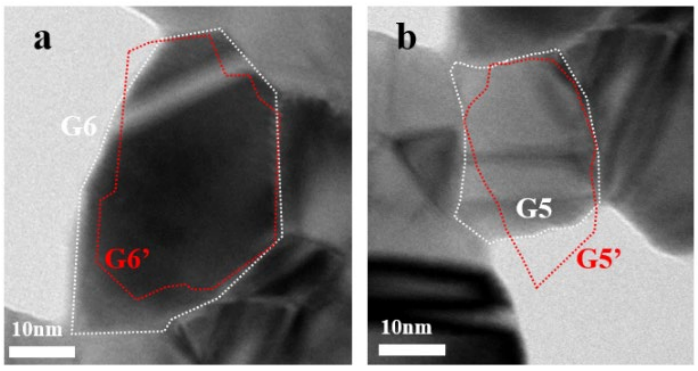

Figure 4.3 Comparisons of the shape/size of G5 and G6 before and after (Figure 4.2f) the deformation, indicating stress-driven GB migration assists GB sliding process. (a) Red dashed line G6' is from Figure 4.1a, the shape/size of G6 is elongated/increased as compared to white dashed line G6. (b) Red dashed line G5' is from Figure 4.2c, the shape/size of G5 is shortened/roughly maintained as compared to white dashed line G5.

It was previously mentioned that the excessive GB slidings easily induce nanovoids nucleation, leading to fast crack propagation in nc-metals. For example, as shown in Figure 4.1, nanocrack nucleated at TJ due to excessive GB sliding. However, in my experimental observations, fewer nanocracks are nucleated as the GB slidings are assisted by stress-driven GB migration. Thus, the stress-driven GB migration process is crucial for the enhanced fracture toughness in nc-Au thin films. Basically, the model of Coble Creep can be referred to account for stress-driven GB migration phenomenon, which follows the formula below[115-117]:

$$e = \frac{14\Omega\sigma D_1}{kTd^2}\left(1 + \frac{\pi W D_{GB}}{D_1 d}\right),$$

where e is the strain rate, Ω=10.2 cm^3/mol is the atomic volume of Au, k=8.3144621 J/(mol·K)) is the Boltzmann's constant, T=333.13 K is the absolute temperature at deformation and d is the grain size, other parameters require further estimation. Referring to Okkerse et al[118], at T=333K (≈0.25 T_m), lattice diffusional coefficient D_l=0.031exp(-39360/kT)=4.54 x 10^{-30} m^2/s. At the same time, GB diffusional coefficient D_{GB}=1.7 x 10^{-21} m^2/s, referring to Würschum et al[119]. Also referring to previous studies[119-121], diffusional coefficient of nc metals should be 2~3 orders of magnitude higher than cg-metals, so finally taking D_l=4.54 x $10^{-27}$$m^2$/s, D_{GB}= 1.7 x 10^{-18} m^2/s. Estimated stress σ≈0.14 ~ 0.43 GPa and GB thickness W≈ 0.5nm, referring to Wang et al[59].

Taking stress-driven GB migration assisted GB slidings along $G_{4\text{-}5}$ in Figure 4.2 as an example, where the total grain size of G5 increases from d=28nm in Figure 4.2a to d=32nm in Figure 4.2f. Based on the data, Coble Creep rate is figured out e ≈ (5.9~26.4) x 10^{-4} s^{-1}. The average localized deformation strain rate is approximately 8.1 x 10^{-4} s^{-1} (see calculations in Figure 4.4), consistent with the Coble Creep rate. Thus, rapid diffusional Coble Creep processes can timely help recover the nanocracks nucleate at TJs in spite of excessive GB slidings.

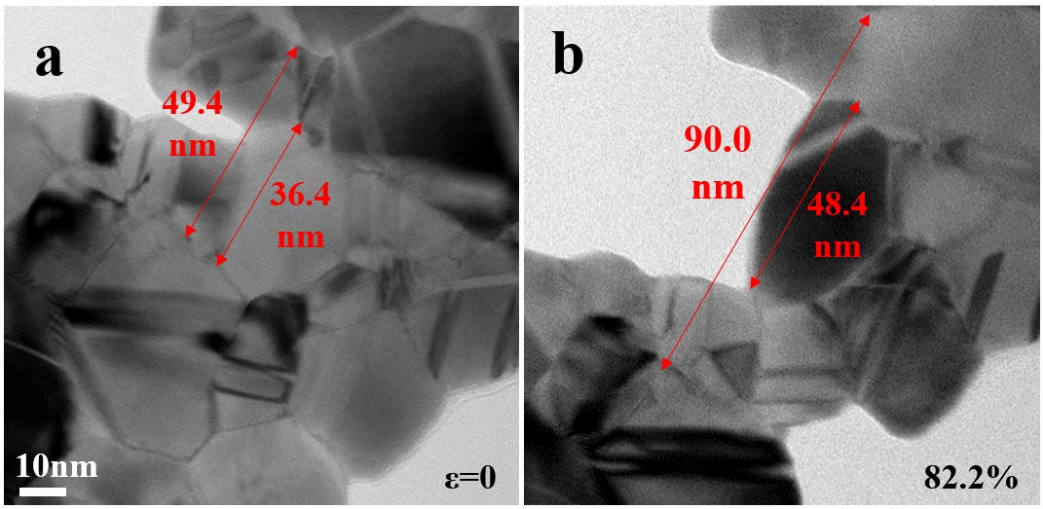

Figure 4.4 Rough calculation of the average localized strain rate of GB slidings along $GB_{4\text{-}5}$ (as shown in Figure 4.2). Strain is 0.822 (shown at the right bottom corner), deformation time was approximately 17min=1020s. Thus, the average strain rate is $0.822/1020s=8.1 \times 10^{-4}\ s^{-1}$.

Figure 4.5 is also a set of partial enlarged TEM images to demonstrate more details of stress-driven GB migration assisted GB slidings. Figure 4.5a exhibits the deformation process subsequent to Figure 4.2. Likewise, the grains are named as "G4~G8". As shown in Figure 4.5a, with tensile straining, GB sliding is along $GB_{4\text{-}6}$ parallel to tensile direction. To track the shape/size changes of G6 before and after straining, boundaries of G6 is highlighted with red dashed lines. With further loading, more GB slidings are along $GB_{4\text{-}6}$, but the GB sliding direction has slightly changed, as shown by red arrows in Figure 4.5b. Subsequently in Figure 4.5c ~ f, more GB slidings perform along $GB_{4\text{-}6}$ till fracture. Interestingly, some nano-steps are observed in Figure 4.5e and Figure 4.5f, which directly indicates the stress-driven GB migration during the GB sliding. The shape/size of G6 in Figure 4.5f is highlighted by white dashed lines. Comparing it with the red dashed lines of G6 (extracted from Figure 4.5a) in Figure 4.5f, the stress-driven GB migration in Figure 4.5 only slightly changes the shape of G6, but its grain growth is very limited. Thus, we can understand that, very limited stress-driven GB migration contributes to the GB sliding process in Figure 4.5.

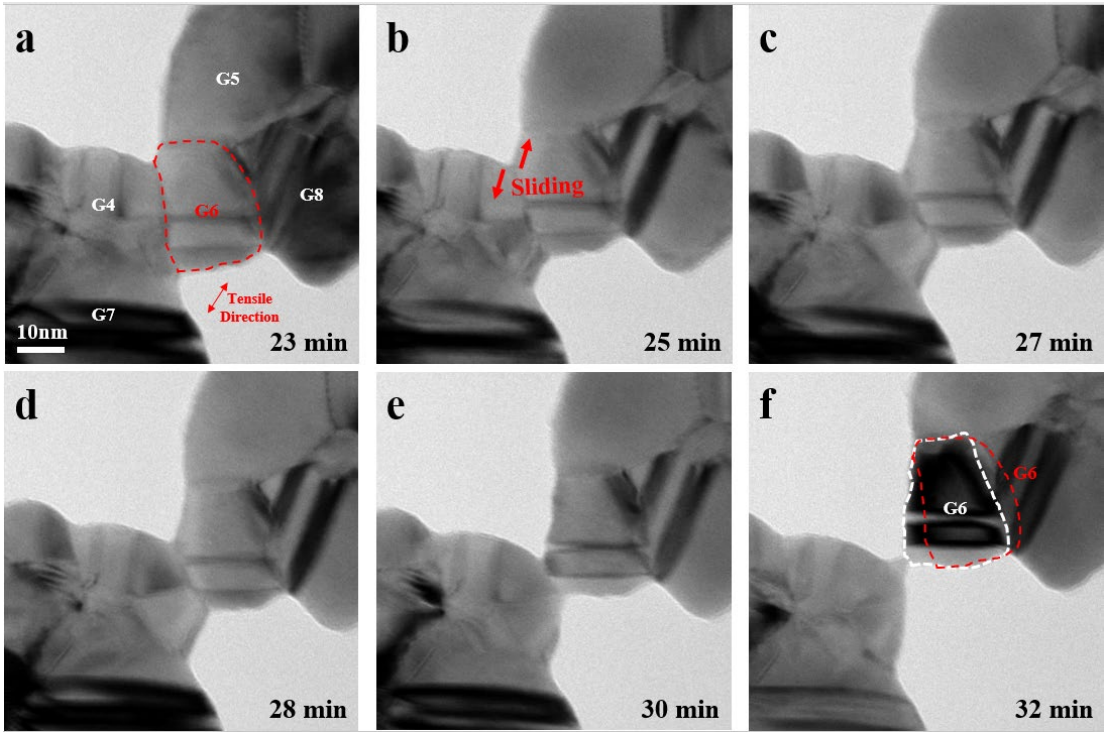

Figure 4.5 Fracture process via GB sliding along $GB_{4\text{-}6}$. The shape/size of G6 in image (a) is highlighted by red dashed lines, and the shape/ size of G6 in image (f) is highlighted by white dashed lines. By comparison of both dashed lines in image (f), the shape of G6 is slightly changed at the moment before fracture, but the size of G6 has minimum changes.

In addition to stress-driven GB migration assisted GB sliding performing at the crack tips (shown Figure 4.2 & Figure 4.5), this cooperative mechanism can also perform along $GB_{6\text{-}7}$ near the crack tips (prior to crack tip propagates to G6), as shown in Figure 4.6. To demonstrate the GB sliding along $GB_{6\text{-}7}$ more clearly, distance between twin lamella "A" of G7 and twin lamella "B" of G6 are highlighted as references. As shown in Figure 4.6, with tensile loading, the distance between twin lamella "A" and twin lamella "B" is reducing from 16.0 nm (shown in Figure 4.6a) to 9.1 nm (shown in Figure 4.6b), 6.6 nm (shown in Figure 4.6c) and finally 5.7 nm (shown in Figure 4.6d). The GB sliding direction in the crack propagation process is approximately parallel to tensile direction, as shown in Figure 4.6e. The shape/size of G6 and G7 are changed during the deformation, so the GB sliding along $GB_{6\text{-}7}$ near the crack tips is also assisted by stress-driven GB migration.

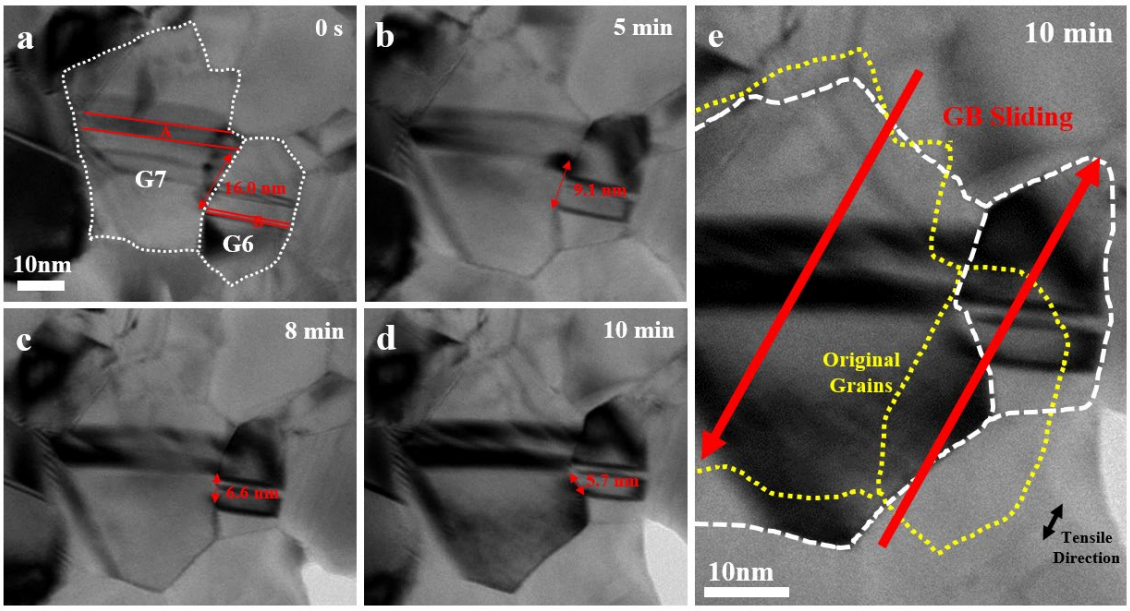

Figure 4.6 In-situ observation of stress-driven GB migration assisted GB sliding process near the crack tip. Distance of twin lamella "A" of G7 and "B" of G6 are measure and compared to indicate GB sliding. From 16.0 nm in image (a), subsequently reduces to 9.1 nm in image (b), 6.6 nm in image (c) and finally 5.7 nm in image (d). (e) The boundaries of G6 and G7 in image (a) are highlighted by yellow dashed lines, compared to boundaries of G6 and G7 in image (d) highlighted by white dashed lines. The shape/size of G6 and G7 are mildly changed, and the GB sliding direction is roughly parallel with tensile direction.

Of all the in-situ observations, some other interesting results for stress-driven GB migration assisted GB slidings are observed. Figure 4.7 exhibits a set of enlarge TEM images, indicating that stress-driven GB migration not only assists smooth GB sliding process between grains but also causes the grains to entirely absorb their "sandwiched" grain. As shown in Figure 4.7a, the crack has already blunted on G1 via GB sliding. Also for convenience, grains are named as "G1~G5" to track their subsequent motions. Boundaries of G1~G3 in Figure 4.7a are marked by using white dashed lines to trace their shape/size changes. With further straining, as shown in Figure 4.7b~d, the crack continuously blunts along $GB_{2\text{-}4}$ and $GB_{3\text{-}5}$. Comparably to G5 in Figure 4.2a~c, G2 and G3 in Figure 4.7b~d are constantly elongated parallel with tensile direction during the deformation, the GB slidings along $GB_{2\text{-}4}$ and $GB_{3\text{-}5}$ are assisted by stress-driven GB migration. Interestingly, it is observed that the "sandwiched" grain G1 is eventually

absorbed by G2 and G3 via stress-driven GB migration during the deformation, the process is as shown in Figure 4.7a~c. Furthermore, as shown in the entire Figure 4.7, the tip of G6 has been also absorbed by G2 and G3 during the GB sliding. Thus, we can understand that stress-driven GB migration and GB sliding can strongly cooperate and accommodate with each other during the crack blunt deformation.

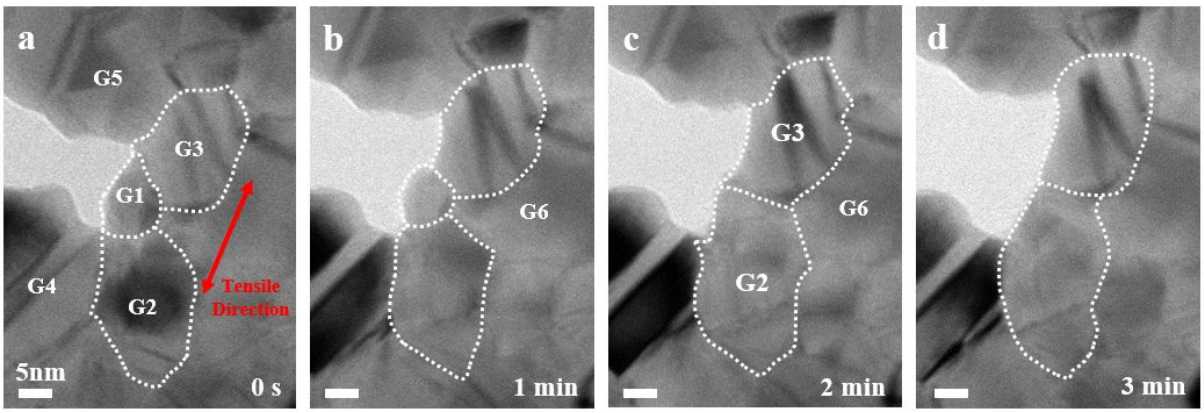

Figure 4.7 In-situ observations of more stress-driven GB migration assisted GB slidings. Under localized tensile stress, GB slidings along $GB_{2\text{-}4}$ and $GB_{3\text{-}5}$ lead the blunted crack to continuously blunt, and the stress-driven GB migration not only assisted the GB slidings and but also simultaneously lead G2 and G3 to "expand" larger via totally absorbing their "sandwiched" grain G1 and partially absorbing the bottom grain G6.

As previously shown in Figure 4.1 ~ Figure 4.7, stress-driven GB migration assisted GB slidings were fundamentally demonstrated and discussed. To show more stress-driven GB migration assisted GB slidings in which other cooperative mechanisms coexist, Figure 4.8~ Figure 4.10 will be further given and discussed.

Figure 4.8 exhibits a set of enlarged TEM images, indicating that grain coalescence eventually takes place, accompanying with stress-driven GB migration assisted GB slidings. Also for convenience, grains are named as "G1~G6" to track their subsequent motions. As shown in Figure 4.8a, a sub-crack tip propagates to G1. Boundaries of G1, G2, G5 and G6 are marked by using white dashed lines. G3 and G4 are two relatively large nanotwinned grains located on both sided of G1, more details are given in Figure 4.9a. With the localized tensile

stress on G1, as shown in Figure 4.8b~c, the crack tip blunts continuously on G1, parallel with tensile direction. At the moment, boundaries of G1, G2 and G5 are marked by red dash lines in Figure 4.8c. With comparing the changes of G1's boundaries in Figure 4.8c (marked by red and white dashed lines), G1 expands to absorb G6. Consequently, G5 becomes the adjacent grain of G1 in Figure 4.8c. In contrast, with comparisons of G2's boundaries, the shape/size of G2 roughly maintains the same. In the deformation process of Figure 4.8a~c, relative position changes of G3 and G4 are shown in Figure 4.9b. It is confirmed that this deformation process is also dominated by stress-driven GB migration assisted GB sliding. Subsequently in Figure 4.8d, with continuing loading, it is observed that G1 coalesces with G2. Boundaries of the new G1 is marked by using yellow dashed lines in Figure 4.8d. Based on the previously reviewed articles, grain coalescence was achieved between nc-Pt grains via grain tilting/ grain rotation and subsequent GB annihilation[35]. With further loading, as shown in Figure 4.8e~f, the wide blunted crack starts to rupture through $GB_{1\text{-}3}$ rather than further crack blunt, and finally the new crack tip propagates to G5. The separation process between G1 and G3 was also accompanied by stress-driven GB migration as the shape/size of G5 moderately is changed. The size of G1 is measured in Figure 4.8c and Figure 4.8d, respectively. Increased from approximately d=16nm to 24nm, size of G1 is instantly enlarged by grain coalescence. It suggests that excessive grain coalescence could be detrimental to stress-driven GB migration assisted GB slidings in straining nc-Au thin films.

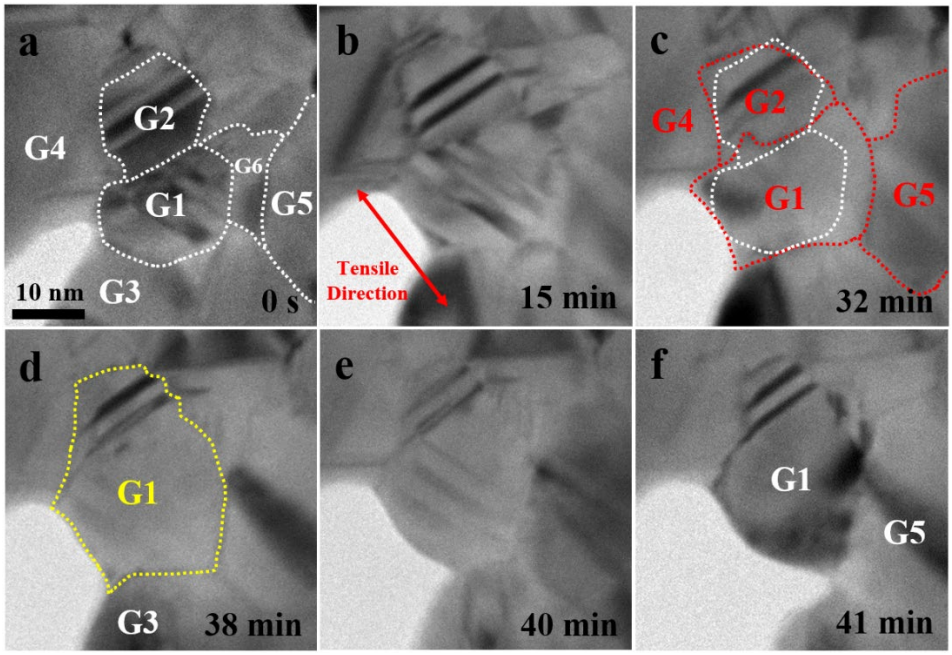

Figure 4.8. In-situ observations of grain coalescence accompanies with stress-driven GB migration assisted GB slidings. (a~c) Under the localized tensile stress, the crack tip blunts by stress-driven GB migration assisted GB slidings. (d) The continuous localized tensile stress drives G1 to coalesce with G2 in which G1 becomes a much larger grain. (e~f) After grain coalescence, a new crack tip develops and propagates through $GB_{1\text{-}3}$ to G5.

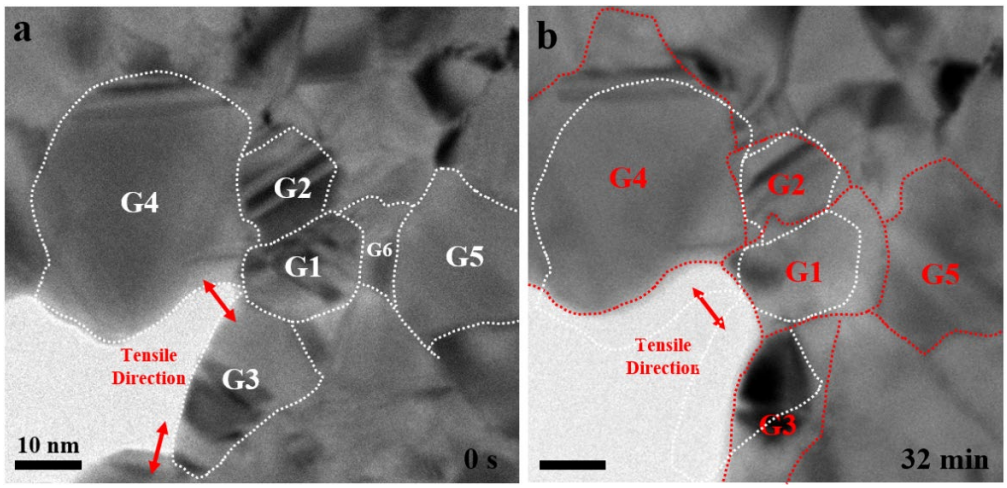

Figure 4.9 (a) Two sub-crack tips are seen on G3. The localized tensile stress directions are marked by red arrows. G1~G5 were all nanotwinned grains. Boundaries of G1~G5 were marked by white dashed lines. G6 is in the middle between G1 and G5. (b) The sub-crack tip on G1 blunts slowly. The boundaries of G1~G5 are marked by red dashed lines. Observing the shape/size/position changes of G1~G4 between (a) and (b) by comparing white dashed lines and red dashed lines, it is confirmed that stress-driven GB migration assisted GB slidings dominate. G1 and G5 became adjacent grains as G1 totally absorbed G6.

Figure 4.10 exhibits a set of enlarged TEM images for another crack blunt process, indicating that GB migration assisted GB sliding is accompanying with GBs-emission partial dislocations and nanotwins nucleation. As shown in Figure 4.10a, the crack tip is on the G1 in which a few defects pre-exist (marked by red arrows). The grains located at the crack tips are named as "G1~G3" and grains located near the crack tips are named as "G4~G8". Boundaries of G1~G5 are marked by using white dashed lines. With tensile loading, the crack tip blunts via GB slidings, so more free surfaces are created on G1. Those initial defects can easily escape from the new-created free surface of G1. Consequently, G1 is quickly free of dislocation, as shown in Figure 4.10b. As shown in Figure 4.10c, with further loading, partial dislocations start to emit from GBs along $GB_{1\text{-}3}$ (highlighted by red dashed line). Subsequently, more partial dislocations nucleate, which eventually evolve into nanotwins, as shown in Figure 4.10d~f. Overall in this crack blunt process, G1 is growing larger and longer by absorbing adjacent grains, obviously stress-driven GB migration assisted GB slidings dominate the deformation. Moreover, GBs-emitted partial dislocations are active and simultaneously accompanying with stress-driven GB migration assisted GB slidings deformation process. However, the specific interacted mechanisms between GBs-emission partial dislocations, nanotwins nucleation and stress-driven GB migration assisted GB sliding are not investigated so that this issue remains unclear. It requires further atomic-scale in-situ investigations on this unsettled issue.

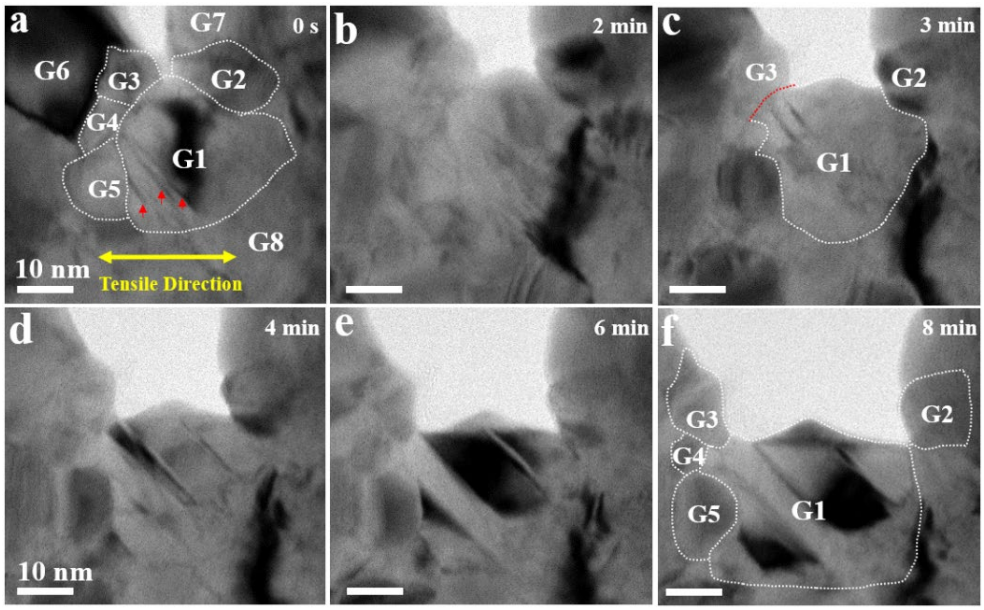

Figure 4.10 Stress-driven GB migration assisted GB sliding is accompanied by partial dislocations emission from GBs and nanotwins generation. (a) The crack tip propagates to G1. Some defects pre-exist in G1, marked by red arrows. (b) With tensile loading, the crack tip blunts along G1. The pre-existed defects escape from the free surface created by crack blunts. (c) With continuous crack blunting parallel with tensile direction, partial dislocations emit from GBs between G1 and G3. (d~f) With continuous crack blunt, more partial dislocations emit from GBs, which eventually evolve into multi-nanotwins.

These in-situ observation results are consistent with the previous MD simulation results and theoretical prediction results. Both Swygenhoven et al[41] and Hasnaoui et al[33] simulated that GB sliding could cooperate with stress-driven GB migration and GBs-emitted partial dislocations; Furthermore, Ovid'ko et al[64] has theoretically modelled cooperative deformation mode of stress-driven GB migration with GB sliding evolved from the crack tips can significantly enhance the fracture toughness of nc-metals, compared to the pure GB slidings; The observation of GB sliding near the crack tip (along $GB_{6\text{-}7}$ in Figure 4.6) is consistent with the predicted model by Bobylev et al[63].

Figure 4.11 are the anticipated schematic diagrams of stress-driven GB migration assisted GB sliding at the crack tips and near the crack tips, based on previously shown Figure 4.1 ~ Figure 4.10. The schematic deformation system consists of 11 smallest grains that are named as

"G1~G11", as shown in Figure 4.11a. With vertical tensile loading, the crack generates and propagates through $G_{2\text{-}3}$ to G6, as shown in Figure 4.11b. With further loading, the crack tip blunts bilaterally along G6, as shown in Figure 4.11c. The shape/size of G2, G3 and G6 have obvious changes in order to accommodate the crack blunting processes. In terms of the real observations (shown in Figure 4.1~4.10), grain size of G2, G3 and G6 can be either increasing or reducing, depending on whether they are nanotwinned grains. More details are shown and discussed later in Figure 4.12. Meanwhile, stress-driven GB migration assisted GB slidings can also be activated near the crack tips, including along $GB_{1\text{-}7}$, $GB_{2\text{-}7}$, $GB_{3\text{-}5}$, $GB_{4\text{-}5}$, $GB_{7\text{-}8}$ and $GB_{5\text{-}11}$ to accommodate the crack blunting process. As the consequence of nucleating fewer nanocracks at TJs, these stress-driven GB migration assisted GB sliding processes near the crack tip are beneficial for enhanced fracture toughness in nc-Au thin films.

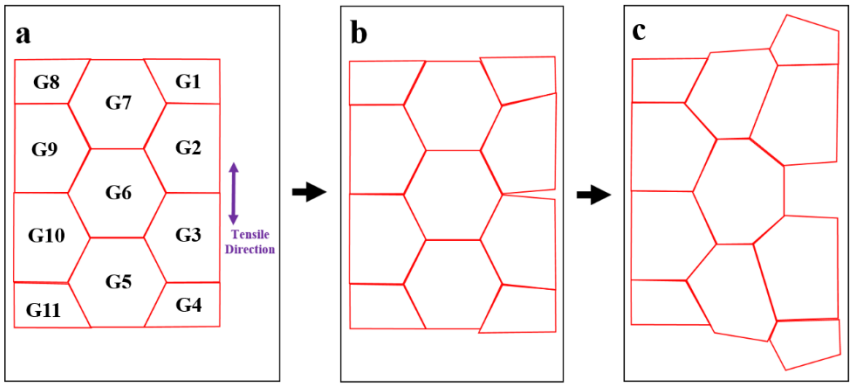

Figure 4.11 Schematic diagrams of the stress-driven GB migration assisted GB sliding at the crack tip and near the crack tip. (a) The smallest grains are named "G1~G11", the tensile direction is vertical. (b) The crack tip generates and propagates through $GB_{2\text{-}3}$ to G6. (c) The crack tip blunts along G6.

During the in-situ experiments, it is observed a number of nanotwinned grains involving in the crack propagation processes, including the nanotwinned grains previously shown in the Figure 4.1 ~ 4.10. In these crack propagation processes, the shape/size of most nanotwinned grains are extended to be longer/larger. To understand the potential relationships between nanotwinned grains and stress-driven grain growth in the crack blunting processes, statistics

are made based on a number of our in-situ observations. As a statistics related to crack propagation processes, it's critically important to identify the crack blunting process and crack rupture process from the crack propagation processes. Basically, this task can be simply figured out by comparing the localized tensile stress direction with the growing crack tip propagation direction: the crack propagation direction of the crack blunting process is approximately parallel with the tensile stress direction, whereas the crack propagation direction of the crack rupture process is approximately perpendicular to the tensile stress direction. For example, as shown in Figure 4.1a~d, the crack propagation direction of the crack 2 along $GB_{8\text{-}9}$ is approximately perpendicular to the localized tensile stress direction, thus it can be identified as crack rupture process; In contrast, as shown in Figure 4.2b~c, the crack propagation direction along $GB_{6\text{-}9}$ of the crack 2 is approximately parallel with the localized tensile direction, thus it can be identified as crack blunting process.

In the statistics, approximately 60 grains are monitored located at the blunting crack tips (could be the stress concentration areas). Statistically, the size of these monitored grains are both measured before the crack tips start to blunt and after the crack tips have already perfectly blunted as far as they can. By comparisons, grain size changes for these monitored grains are obtained. Simultaneously, it is also monitored that whether these grains contained nanotwins. The existence of nanotwins can be pre-existed inside the grains or alternatively they nucleate inside the grains during the crack blunting processes. Combining all these statistic data, Figure 4.12a shows a scatter diagram, indicating the tendency of stress-driven grain growth at the blunting crack tips. The horizontal axis of Figure 4.12a shows the grain size distribution before the crack tips start to blunt, the vertical axis shows the grain size changes during the crack tips blunting processes and the red/green dots indicates they are nanotwinned/none-nanotwinned grains during the crack blunting processes. As shown in Figure 4.12a, it is clearly discovered that grain size range of the monitored grains dominantly distributes from 10 nm to 30nm.

Interestingly, it is also discovered that most of the nanotwinned grains located at the crack tips grow into larger size during the crack blunting processes, a few of them even have significant growths. However, in contrast, most of the rest of none-nanotwinned grains located at the crack tips shrink into smaller size during the crack blunting processes. The amount of grain shrinkage is statistically limited by 4 nm for each grain. Thus, the tendency of none-nanotwinned grains shrinkage is not as significant as the nanotwinned grains growth. Based on Figure 4.12a, it indicates that nanotwinned grains located at the blunting crack tips could tend to absorb parts of their adjacent none-nanotwinned grains located at the blunting crack tips.

Meanwhile, to compare with Figure 4.12a, more 60 grains located near the blunting crack tips are also monitored. The description of "near the blunting crack tips" means that the statistical grains are not exactly located at the blunting crack tips, but they are much closed to the blunting crack tips. For example, as shown in the Figure 4.2a, G4 and G5 are located at the blunting crack tips, whereas G6, G7 and G10 are located near the blunting crack tips. Comparing to the grains located at the crack tips, the grains located near the crack tips are still at tensile stress but could not on stress concentration. In those "near the blunting crack tips" areas, the grain size changes and existence of naotwins for these 60 grains are also monitored. Combing the statistics data, Figure 4.12b shows a scatter diagram, indicating the tendency of grain size changes near the blunting crack tips. The horizontal/vertical axis and red/green dots of Figure 4.12b represent the same meanings as Figure 4.12a. As shown in Figure 4.12b, it is discovered that grain size range of the monitored grains dominantly distributes from 0 nm to 20nm, roughly consistent with the grain size statistics in Figure 3.2. Comparing to Figure 4.12a, the grain size of the grains located near the crack tips was slightly smaller than the grains located at the crack tips. Interestingly, it is also discovered that most of the grains with grain size smaller than 10 nm, even with slightly bigger size 10.2nm, were entirely absorbed by adjacent grains during the crack blunting processes, indicated by the linear dashed line passing through

the origin point. These "tiny-grain disappearances" could significantly contribute to the stress-driven grain growth of the nanotwinned grains located at the crack tips (shown in Figure 4.12a). Differently from Figure 4.12a, the tendency of grain size changes of the grains near the blunting crack tips are random and independent to the existence of nanotwins. Thus, apart from none-nantwinned grains located at the blunting crack tips, any adjacent grains near the blunting crack tips are the potential "resources" for the stress-driven grain growth of nanotwinned grains located at the blunting crack tips.

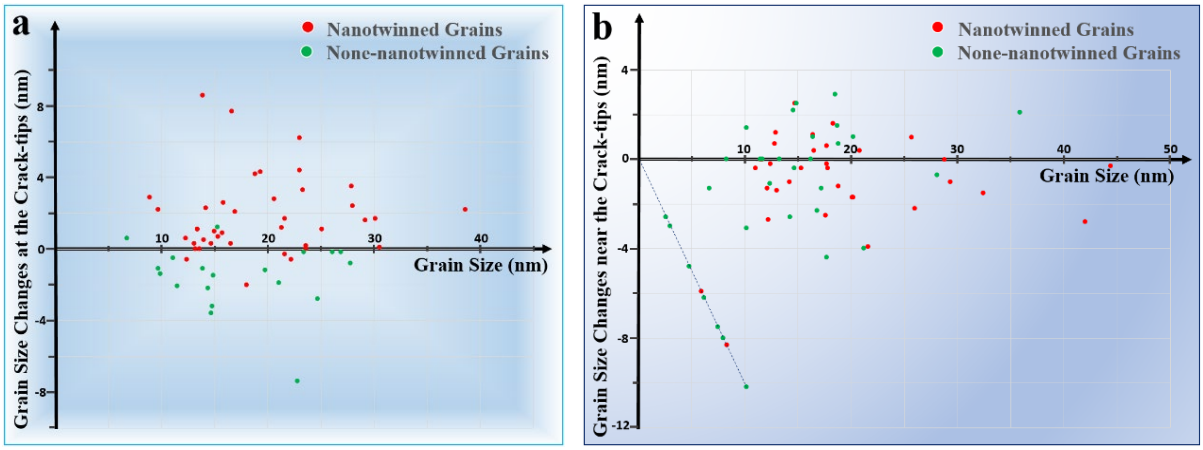

Figure 4.12 (a) Statistical data of grain size changes at the blunting crack tips versus initial grain size of these grains before crack tips start to blunt. For all these grains, nanotwinned grains are marked by red dots and none-nanotwinned grains are marked by green dots. During crack tips blunt, grain size of most nanotwinned grains increase but in contrast none-nanotwinned grains decreased. (b) Statistical data shows the tendency of grain size changes near the blunting crack tips. Most grains with d<10nm (even d=10.2nm) are totally absorbed by the adjacent grains during crack tip blunt. The tendency of grain growths near the blunting crack tips are independent to the existence of nanotwins.

Previous study by Luo et al [111] can be referred to understand the stress-driven grain growth tendency discovered in the statistical studies of Figure 4.12. In Luo's study, fatigue tests are performed on the nc-Au thin films (with thickness ~ 20 nm, average grain size ~ 19.0 nm). After repeating cyclic tensile loadings, the grain size statistics results exhibit that the average grain size of the fatigued nc-Au thin films significantly increases to 41.3 nm. Therein, the

original nanotwinned grains have stronger tendencies to be coarsened mechanically, and the multi-twins nucleation processes are frequently found in these enlarging nanotwinned grains. Meanwhile, the statistics results discover that the number of nanotwinned grains increases significantly in the fatigued nc-Au thin films, indicating that the nanotwins nucleation is positively correlated to the stress-driven grain growth. Therefore, the existence/ nucleation of nanotwins could also promote the stress-driven grain growth on the Luo's nc-Au thin films. Different from the fatigue tests of Luo's study, our nc-Au thin films are experiencing higher tensile stress which leads to quicker crack propagation processes. Especially for the grains located at the crack tips, stress concentration could be performing on these grains. As we know that nanotwinned grains are sensitive to the applying stress, the nanotwinned grains located at the blunting crack tips could be implemented more stress stimulations and consequently show stronger tendencies of stress-driven grain growth.

Chapter 5. Conclusion, Limitation & Future Outlook

5.1 Conclusions

In this study, with utilising the homemade TEM tensile device and TEM heating holder, in-situ TEM tensile experiments have been conducted on the PVD-fabricated nc-Au thin films. From the observations of crack propagation processes, it has been confirmed that GB sliding and stress-driven GB migration are the cooperative mechanisms for the straining nc-Au thin films, consistent with the previous studies of theoretical predictions and MD simulations. Nucleating fewer nanocracks during GB slidings located at the crack tips and located near the crack tips, cooperation of stress-driven GB migration and GB slidings can assist to achieve enhanced ductility. In addition, grain coalescence and partial dislocations emitted from the GBs are occasionally accompanying with the stress-driven GB migration and GB sliding cooperative mechanisms. Furthermore, it is statistically discovered that the nanotwinned grains

located at the blunting cracks tend to experience stress-driven grain growth. In contrast, the tendency of grain growth near the blunting crack tips are independent to the existence of nanotwins. Interestingly, the smallest grains (d<10nm) near the blunting cracks tend to be totally absorbed by their adjacent larger grains, which can be a contributor to the tendency of stress-driven nanotwinned grain growth at the crack tips.

5.2 Limitation

In this study, during the in-situ TEM experiments, objective aperture in the operated TEM was always inserted by the smallest size aperture. Unambiguous GBs motions have been observed and recorded by using this TEM brightest field mode. However, occasionally a few GBs are difficult to be identified and confirmed from other line features such as long full dislocations and sample distorted contrast. Aiming at this difficulty, high-resolution TEM (HRTEM) mode is one of the best solutions. However, unfortunately, no in-situ HRTEM observation was accomplished during my experiments. Meanwhile, my observations are so emphasized on GBs motions (ignored dislocations activities) that it is difficult to draw any conclusion on the relationship between GBs motions and full dislocations/ partial dislocations activities. Although full dislocations are rare in the nc-Au thin films, they are still observed during the deformation processes (in larger grains, full dislocations sometimes nucleate and escape during the crack blunting processes).

5.3 Future Outlook

So far, a number of studies have intensively investigated GBs-mediated mechanisms and partial dislocation mediated mechanisms (or twinning mechanisms) in nc-metals, but few previous studies combined both together and investigated their relationships and interactions during the deformation. Like Figure 4.10 and my other observations, active partial dislocation activities are occasionally observed during the crack blunting processes. The stress-driven migration assisted GB slidings are accompanied by the simultaneous process of continuous

partial dislocations GBs-emissions and the subsequent nanotwins nucleation. To deeper understand their relationships, interactions and impacts on the deformation processes of nc-Au thin films, more in-situ HRTEM experiments are required.

In this study, meanwhile, only nc-Au thin films with thickness ~ 15nm are experimentally studied. As introduced in the previous sections, we understand that size effect can produce huge impact on the mechanical performances and deformation mechanism of the nanocrystalline metallic films, including film thickness effect. Therefore, with utilising our homemade tensile device, further investigations should also be emphasized on the film thickness effect of the deformation mechanisms of nc-Au thin films. For example, nc-Au thin films with thickness 5nm, 10nm, 15nm, 20nm, 25nm, 30nm and 50nm can be fabricated by adjusting the parameters of magnetic sputtering. Subsequently, in-situ TEM straining experiments can be carried out on these fabricated nc-Au thin films (with different thickness), and the obtained experimental observations will show different deformation mechanisms that take place on these nc-Au thin films with different thickness. Finally, statistics can be made to discover whether deformation mechanism transition phenomenon could also be existent in these nc-Au thin films, attributed to the film thickness effect.

Reference

1 Callister, W. D. & Rethwisch, D. G. *Fundamentals of materials science and engineering*. Vol. 471660817 (Wiley London, UK:, 2000).
2 Shackelford, J. F. & Muralidhara, M. K. Introduction to materials science for engineers. (2005).
3 Smith, W. F. & Hashemi, J. *Foundations of materials science and engineering*. (McGraw-Hill, 2011).
4 Stefanescu, D. M. *Science and engineering of casting solidification*. (Springer, 2015).
5 Hirth, J. P., Lothe, J. & Mura, T. (American Society of Mechanical Engineers, 1983).
6 Yip, S. Nanocrystals: the strongest size. *Nature* **391**, 532 (1998).
7 Argon, A. & Yip, S. The strongest size. *Philosophical magazine letters* **86**, 713-720 (2006).
8 Schiøtz, J., Di Tolla, F. D. & Jacobsen, K. W. Softening of nanocrystalline metals at very small grain sizes. *Nature* **391**, 561 (1998).

9 Schiøtz, J. & Jacobsen, K. W. A maximum in the strength of nanocrystalline copper. *Science* **301**, 1357-1359 (2003).
10 Carlton, C. & Ferreira, P. What is behind the inverse Hall–Petch effect in nanocrystalline materials? *Acta Materialia* **55**, 3749-3756 (2007).
11 Fan, G., Choo, H., Liaw, P. & Lavernia, E. A model for the inverse Hall–Petch relation of nanocrystalline materials. *Materials Science and Engineering: A* **409**, 243-248 (2005).
12 Padmanabhan, K., Dinda, G., Hahn, H. & Gleiter, H. Inverse Hall–Petch effect and grain boundary sliding controlled flow in nanocrystalline materials. *Materials science and Engineering: A* **452**, 462-468 (2007).
13 Van Swygenhoven, H. & Weertman, J. R. Deformation in nanocrystalline metals. *Materials today* **9**, 24-31 (2006).
14 Schiøtz, J. Atomic-scale modeling of plastic deformation of nanocrystalline copper. *Scripta Materialia* **51**, 837-841 (2004).
15 Yamakov, V., Wolf, D., Phillpot, S., Mukherjee, A. & Gleiter, H. Deformation mechanism crossover and mechanical behaviour in nanocrystalline materials. *Philosophical Magazine Letters* **83**, 385-393 (2003).
16 Zhu, B., Asaro, R., Krysl, P. & Bailey, R. Transition of deformation mechanisms and its connection to grain size distribution in nanocrystalline metals. *Acta Materialia* **53**, 4825-4838 (2005).
17 Meyers, M. A., Mishra, A. & Benson, D. J. The deformation physics of nanocrystalline metals: Experiments, analysis, and computations. *Jom* **58**, 41-48 (2006).
18 Kumar, K., Van Swygenhoven, H. & Suresh, S. Mechanical behavior of nanocrystalline metals and alloys1. *Acta Materialia* **51**, 5743-5774 (2003).
19 Chen, B. *et al.* Texture of nanocrystalline nickel: Probing the lower size limit of dislocation activity. *Science* **338**, 1448-1451 (2012).
20 Chen, M. *et al.* Deformation twinning in nanocrystalline aluminum. *Science* **300**, 1275-1277 (2003).
21 Liao, X. *et al.* Deformation mechanism in nanocrystalline Al: Partial dislocation slip. *Applied Physics Letters* **83**, 632-634 (2003).
22 Liao, X. *et al.* Deformation twinning in nanocrystalline copper at room temperature and low strain rate. *Applied physics letters* **84**, 592-594 (2004).
23 Liao, X., Zhou, F., Lavernia, E., He, D. & Zhu, Y. Deformation twins in nanocrystalline Al. *Applied physics letters* **83**, 5062-5064 (2003).
24 Yamakov, V., Wolf, D., Phillpot, S. & Gleiter, H. Deformation twinning in nanocrystalline Al by molecular-dynamics simulation. *Acta Materialia* **50**, 5005-5020 (2002).
25 Zhu, Y., Liao, X. & Wu, X. Deformation twinning in nanocrystalline materials. *Progress in Materials Science* **57**, 1-62 (2012).
26 Yamakov, V., Wolf, D., Salazar, M., Phillpot, S. & Gleiter, H. Length-scale effects in the nucleation of extended dislocations in nanocrystalline Al by molecular-dynamics simulation. *Acta Materialia* **49**, 2713-2722 (2001).
27 Zhu, Y. *et al.* Nucleation and growth of deformation twins in nanocrystalline aluminum. *Applied physics letters* **85**, 5049-5051 (2004).
28 Wu, X. *et al.* New deformation twinning mechanism generates zero macroscopic strain in nanocrystalline metals. *Physical review letters* **100**, 095701 (2008).
29 Wu, X., Zhu, Y., Chen, M. & Ma, E. Twinning and stacking fault formation during tensile deformation of nanocrystalline Ni. *Scripta Materialia* **54**, 1685-1690 (2006).
30 Rösner, H., Markmann, J. & Weissmüller, J. Deformation twinning in nanocrystalline Pd. *Philosophical magazine letters* **84**, 321-334 (2004).

31 Gianola, D. *et al.* Stress-assisted discontinuous grain growth and its effect on the deformation behavior of nanocrystalline aluminum thin films. *Acta Materialia* **54**, 2253-2263 (2006).
32 Farkas, D., Frøseth, A. & Van Swygenhoven, H. Grain boundary migration during room temperature deformation of nanocrystalline Ni. *Scripta Materialia* **55**, 695-698 (2006).
33 Hasnaoui, A., Van Swygenhoven, H. & Derlet, P. Cooperative processes during plastic deformation in nanocrystalline fcc metals: A molecular dynamics simulation. *Physical Review B* **66**, 184112 (2002).
34 Liu, P., Mao, S., Wang, L., Han, X. & Zhang, Z. Direct dynamic atomic mechanisms of strain-induced grain rotation in nanocrystalline, textured, columnar-structured thin gold films. *Scripta Materialia* **64**, 343-346 (2011).
35 Wang, L. *et al.* Grain rotation mediated by grain boundary dislocations in nanocrystalline platinum. *Nature communications* **5**, 4402 (2014).
36 Ke, M., Hackney, S., Milligan, W. & Aifantis, E. Observation and measurement of grain rotation and plastic strain in nanostructured metal thin films. *Nanostructured Materials* **5**, 689-697 (1995).
37 Legros, M., Gianola, D. S. & Hemker, K. J. In situ TEM observations of fast grain-boundary motion in stressed nanocrystalline aluminum films. *Acta Materialia* **56**, 3380-3393 (2008).
38 Haslam, A. *et al.* Stress-enhanced grain growth in a nanocrystalline material by molecular-dynamics simulation. *Acta Materialia* **51**, 2097-2112 (2003).
39 Haslam, A., Phillpot, S., Wolf, D., Moldovan, D. & Gleiter, H. Mechanisms of grain growth in nanocrystalline fcc metals by molecular-dynamics simulation. *Materials Science and Engineering: A* **318**, 293-312 (2001).
40 Moldovan, D., Yamakov, V., Wolf, D. & Phillpot, S. R. Scaling behavior of grain-rotation-induced grain growth. *Physical review letters* **89**, 206101 (2002).
41 Van Swygenhoven, H. & Derlet, P. Grain-boundary sliding in nanocrystalline fcc metals. *Physical Review B* **64**, 224105 (2001).
42 Jin, M., Minor, A., Stach, E. & Morris Jr, J. Direct observation of deformation-induced grain growth during the nanoindentation of ultrafine-grained Al at room temperature. *Acta Materialia* **52**, 5381-5387 (2004).
43 Sansoz, F. & Dupont, V. Grain growth behavior at absolute zero during nanocrystalline metal indentation. *Applied Physics Letters* **89**, 111901 (2006).
44 Gutkin, M. Y., Ovid'ko, I. & Skiba, N. Crossover from grain boundary sliding to rotational deformation in nanocrystalline materials. *Acta Materialia* **51**, 4059-4071 (2003).
45 Harris, K., Singh, V. & King, A. Grain rotation in thin films of gold. *Acta materialia* **46**, 2623-2633 (1998).
46 Zhang, K., Weertman, J. & Eastman, J. Rapid stress-driven grain coarsening in nanocrystalline Cu at ambient and cryogenic temperatures. *Applied Physics Letters* **87**, 061921 (2005).
47 Ivanisenko, Y. *et al.* Deformation mechanisms in nanocrystalline palladium at large strains. *Acta Materialia* **57**, 3391-3401 (2009).
48 Liu, Y., Zhou, J., Shen, T. & Hui, D. Grain rotation dependent fracture toughness of nanocrystalline materials. *Materials Science and Engineering: A* **528**, 7684-7687 (2011).
49 Trautt, Z. & Mishin, Y. Grain boundary migration and grain rotation studied by molecular dynamics. *Acta Materialia* **60**, 2407-2424 (2012).
50 Monk, J. & Farkas, D. Strain-induced grain growth and rotation in nickel nanowires. *Physical Review B* **75**, 045414 (2007).

51 Tirumalasetty, G. *et al.* Deformation-induced austenite grain rotation and transformation in TRIP-assisted steel. *Acta Materialia* **60**, 1311-1321 (2012).
52 Guo, Y., Wang, J., Wang, Z., Tang, S. & Zhou, Y. Phase field crystal modeling of grain rotation with small initial misorientations in nanocrystalline materials. *Computational Materials Science* **88**, 163-169 (2014).
53 Hibbard, G., Radmilovic, V., Aust, K. & Erb, U. Grain boundary migration during abnormal grain growth in nanocrystalline Ni. *Materials Science and Engineering: A* **494**, 232-238 (2008).
54 Gertsman, V. Y. & Birringer, R. On the room-temperature grain growth in nanocrystalline copper. *Scripta metallurgica et materialia* **30**, 577-581 (1994).
55 Kacher, J., Robertson, I., Nowell, M., Knapp, J. & Hattar, K. Study of rapid grain boundary migration in a nanocrystalline Ni thin film. *Materials Science and Engineering: A* **528**, 1628-1635 (2011).
56 Wang, Y., Li, B., Sui, M. & Mao, S. Deformation-induced grain rotation and growth in nanocrystalline Ni. *Applied Physics Letters* **92**, 011903 (2008).
57 Shan, Z. *et al.* Large lattice strain in individual grains of deformed nanocrystalline Ni. *Applied Physics Letters* **92**, 091917 (2008).
58 Shan, Z. *et al.* Grain boundary-mediated plasticity in nanocrystalline nickel. *Science* **305**, 654-657 (2004).
59 Wang, L. *et al.* In situ observation of stress induced grain boundary migration in nanocrystalline gold. *Scripta Materialia* **134**, 95-99 (2017).
60 Kumar, S., Li, X., Haque, A. & Gao, H. Is stress concentration relevant for nanocrystalline metals? *Nano letters* **11**, 2510-2516 (2011).
61 Wang, Y. *et al.* Mechanism of grain growth during severe plastic deformation of a nanocrystalline Ni–Fe alloy. *Applied Physics Letters* **94**, 011908 (2009).
62 Farkas, D., Mohanty, S. & Monk, J. Linear grain growth kinetics and rotation in nanocrystalline Ni. *Physical review letters* **98**, 165502 (2007).
63 Bobylev, S., Morozov, N. & Ovid'ko, I. Cooperative grain boundary sliding and migration process in nanocrystalline solids. *Physical review letters* **105**, 055504 (2010).
64 Ovid'Ko, I., Sheinerman, A. & Aifantis, E. Effect of cooperative grain boundary sliding and migration on crack growth in nanocrystalline solids. *Acta Materialia* **59**, 5023-5031 (2011).
65 Yamakov, V., Wolf, D., Phillpot, S. & Gleiter, H. Grain-boundary diffusion creep in nanocrystalline palladium by molecular-dynamics simulation. *Acta Materialia* **50**, 61-73 (2002).
66 Wei, Y., Bower, A. F. & Gao, H. Enhanced strain-rate sensitivity in fcc nanocrystals due to grain-boundary diffusion and sliding. *Acta Materialia* **56**, 1741-1752 (2008).
67 Borodin, E. & Mayer, A. A simple mechanical model for grain boundary sliding in nanocrystalline metals. *Materials Science and Engineering: A* **532**, 245-248 (2012).
68 Kumar, K., Suresh, S., Chisholm, M., Horton, J. & Wang, P. Deformation of electrodeposited nanocrystalline nickel. *Acta Materialia* **51**, 387-405 (2003).
69 Sergueeva, A., Mara, N., Krasilnikov, N., Valiev, R. & Mukherjee, A. Cooperative grain boundary sliding in nanocrystalline materials. *Philosophical Magazine* **86**, 5797-5804 (2006).
70 Hosseinian, E., Gupta, S., Pierron, O. N. & Legros, M. Size effects on intergranular crack growth mechanisms in ultrathin nanocrystalline gold free-standing films. *Acta Materialia* **143**, 77-87 (2018).
71 Ovid'ko, I. & Sheinerman, A. Triple junction nanocracks in deformed nanocrystalline materials. *Acta materialia* **52**, 1201-1209 (2004).

72 Ovid'ko, I. & Sheinerman, A. Special strain hardening mechanism and nanocrack generation in nanocrystalline materials. *Applied physics letters* **90**, 171927 (2007).
73 Ovid'Ko, I. Review on the fracture processes in nanocrystalline materials. *Journal of materials science* **42**, 1694-1708 (2007).
74 Ovid'ko, L. & Sheinerman, A. Triple junction nanocracks in fatigued nanocrystalline materials. *Reviews on Advanced Materials Science* **7**, 61-66 (2004).
75 Gutkin, M. Y. & Ovid'ko, I. Nanocracks at grain boundaries in nanocrystalline materials. *Philosophical magazine letters* **84**, 655-663 (2004).
76 Morozov, N., Ovid'ko, I., Petrov, Y. V. & Sheinerman, A. Generation and converence of nanocracks in nanocrystalline materials deformed by grain boundary sliding. *Rev. Adv. Mater. Sci* **19**, 63-72 (2009).
77 Zhao, Y., Fang, Q. & Liu, Y. Effect of cooperative nanograin boundary sliding and migration on dislocation emission from a blunt nanocrack tip in nanocrystalline materials. *Philosophical Magazine* **94**, 700-730 (2014).
78 Frank, F. C. & Mott, N. F. The Frank—Read source. *Proceedings of the Royal Society of London. A. Mathematical and Physical Sciences* **371**, 136-138, doi:doi:10.1098/rspa.1980.0069 (1980).
79 Zhu, Y. *et al.* Dislocation–twin interactions in nanocrystalline fcc metals. *Acta Materialia* **59**, 812-821 (2011).
80 Nie, X., Wang, R., Ye, Y., Zhou, Y. & Wang, D. Calculations of stacking fault energy for fcc metals and their alloys based on an improved embedded-atom method. *Solid state communications* **96**, 729-734 (1995).
81 Crampin, S., Hampel, K., Vvedensky, D. & MacLaren, J. The calculation of stacking fault energies in close-packed metals. *Journal of Materials Research* **5**, 2107-2119 (1990).
82 Johnson, R. Stability of tight-packed metals with the embedded-atom method. *Journal of materials research* **7**, 883-887 (1992).
83 Baskes, M. Modified embedded-atom potentials for cubic materials and impurities. *Physical review B* **46**, 2727 (1992).
84 Li, R. *et al.* Stacking fault energy of face-centered cubic metals: thermodynamic and ab initio approaches. *Journal of Physics: Condensed Matter* **28**, 395001 (2016).
85 Li, X. & Schönecker, S. First-principles prediction of the stacking fault energy of gold at finite temperature. *Acta Materialia* **135**, 88-95 (2017).
86 Van Swygenhoven, H., Derlet, P. & Frøseth, A. Stacking fault energies and slip in nanocrystalline metals. *Nature materials* **3**, 399 (2004).
87 Zimmerman, J. A., Gao, H. & Abraham, F. F. Generalized stacking fault energies for embedded atom FCC metals. *Modelling and Simulation in Materials Science and Engineering* **8**, 103 (2000).
88 Qin, E., Lu, L., Tao, N., Tan, J. & Lu, K. Enhanced fracture toughness and strength in bulk nanocrystalline Cu with nanoscale twin bundles. *Acta Materialia* **57**, 6215-6225 (2009).
89 Singh, A., Tang, L., Dao, M., Lu, L. & Suresh, S. Fracture toughness and fatigue crack growth characteristics of nanotwinned copper. *Acta Materialia* **59**, 2437-2446 (2011).
90 Huang, Q. *et al.* Nanotwinned diamond with unprecedented hardness and stability. *Nature* **510**, 250 (2014).
91 Zhang, Z. *et al.* Ultrahigh hardness and synergistic mechanism of a nanotwinned structure of cadmium zinc telluride. *Scripta Materialia* **68**, 747-750 (2013).
92 Pan, Q., Zhou, H., Lu, Q., Gao, H. & Lu, L. History-independent cyclic response of nanotwinned metals. *Nature* **551**, 214 (2017).

93 Priester, L. *Grain boundaries: from theory to engineering*. Vol. 172 (Springer Science & Business Media, 2012).
94 Wang, L., Zhang, Z., Ma, E. & Han, X. Transmission electron microscopy observations of dislocation annihilation and storage in nanograins. *Applied Physics Letters* **98**, 051905 (2011).
95 Wang, L. *et al.* In situ observation of dislocation behavior in nanometer grains. *Physical review letters* **105**, 135501 (2010).
96 Xu, D. *et al.* Nanotwin formation in copper thin films by stress/strain relaxation in pulse electrodeposition. *Applied Physics Letters* **91**, 254105 (2007).
97 Cai, J., Shekhar, S., Wang, J. & Shankar, M. R. Nanotwinned microstructures from low stacking fault energy brass by high-rate severe plastic deformation. *Scripta materialia* **60**, 599-602 (2009).
98 Christian, J. W. & Mahajan, S. Deformation twinning. *Progress in materials science* **39**, 1-157 (1995).
99 Ookawa, A. On the mechanism of deformation twin in fcc crystal. *Journal of the Physical Society of Japan* **12**, 825-825 (1957).
100 Venables, J. Deformation twinning in face-centred cubic metals. *Philosophical magazine* **6**, 379-396 (1961).
101 Niewczas, M. & Saada, G. Twinning nucleation in Cu-8 at.% Al single crystals. *Philosophical Magazine A* **82**, 167-191 (2002).
102 Yamakov, V., Wolf, D., Phillpot, S. R., Mukherjee, A. K. & Gleiter, H. Dislocation processes in the deformation of nanocrystalline aluminium by molecular-dynamics simulation. *Nature materials* **1**, 45 (2002).
103 Wu, X. & Zhu, Y. Partial-dislocation-mediated processes in nanocrystalline Ni with nonequilibrium grain boundaries. *Applied physics letters* **89**, 031922 (2006).
104 Zhu, Y., Liao, X. & Wu, X. Deformation twinning in bulk nanocrystalline metals: experimental observations. *Jom* **60**, 60 (2008).
105 Zhu, Y. *et al.* Twinning partial multiplication at grain boundary in nanocrystalline fcc metals. *Applied Physics Letters* **95**, 031909 (2009).
106 Wang, L. *et al.* New twinning route in face-centered cubic nanocrystalline metals. *Nature communications* **8**, 2142 (2017).
107 Humphreys, F. J. & Hatherly, M. *Recrystallization and related annealing phenomena*. (Elsevier, 2012).
108 Sharon, J., Su, P., Prinz, F. & Hemker, K. Stress-driven grain growth in nanocrystalline Pt thin films. *Scripta Materialia* **64**, 25-28 (2011).
109 Mompiou, F. *et al.* Inter-and intragranular plasticity mechanisms in ultrafine-grained Al thin films: An in situ TEM study. *Acta materialia* **61**, 205-216 (2013).
110 Yuk, J. M. *et al.* In situ atomic imaging of coalescence of Au nanoparticles on graphene: rotation and grain boundary migration. *Chemical Communications* **49**, 11479-11481 (2013).
111 Luo, X.-M., Zhu, X.-F. & Zhang, G.-P. Nanotwin-assisted grain growth in nanocrystalline gold films under cyclic loading. *Nature communications* **5**, 3021 (2014).
112 Luo, X.-M. & Zhang, G.-P. Deformation-mechanism dependent stretchability of nanocrystalline gold films on flexible substrates. *Journal of Materials Research* **32**, 3516-3523 (2017).
113 Chawla, K. K. & Meyers, M. *Mechanical behavior of materials*. (Prentice Hall Upper Saddle River, 1999).
114 Milligan, W., Hackney, S., Ke, M. & Aifantis, E. In situ studies of deformation and fracture in nanophase materials. *Nanostructured Materials* **2**, 267-276 (1993).

115 Wang, N., Wang, Z., Aust, K. & Erb, U. Room temperature creep behavior of nanocrystalline nickel produced by an electrodeposition technique. *Materials Science and Engineering: A* **237**, 150-158 (1997).
116 Li, Y., Blum, W. & Breutinger, F. Does nanocrystalline Cu deform by Coble creep near room temperature? *Materials Science and Engineering: A* **387**, 585-589 (2004).
117 Coble, R. A model for boundary diffusion controlled creep in polycrystalline materials. *Journal of applied physics* **34**, 1679-1682 (1963).
118 Okkerse, B. Self-diffusion of gold. *Physical Review* **103**, 1246 (1956).
119 Würschum, R., Herth, S. & Brossmann, U. Diffusion in nanocrystalline metals and alloys—a status report. *Advanced engineering materials* **5**, 365-372 (2003).
120 Herzig, C. & Divinski, S. V. Grain boundary diffusion in metals: recent developments. *Materials Transactions* **44**, 14-27 (2003).
121 Kaur, I., Mishin, Y. & Gust, W. *Fundamentals of grain and interphase boundary diffusion*. (John Wiley, 1995).

Appendice

Appendix 1

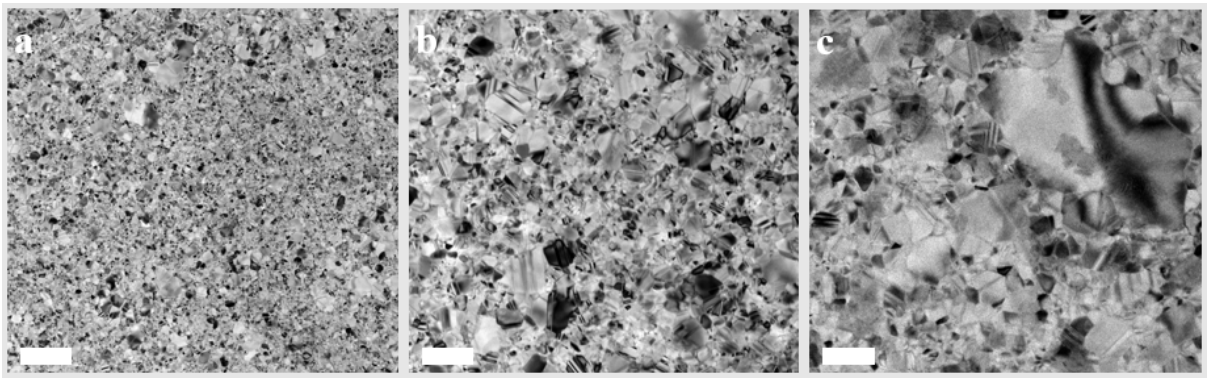

TEM images of different magnification that show the morphology of the fabricated nc-Au thin films, few nanocracks/ nanovoids can be observed. Scale bar: (a) 200nm, (b) 100nm, (c) 50nm.